A Multi-Method Antarctic Atmospheric Blocking Dataset (1979-2024)

Deniz Bozkurt[1,2,3], Charlie Opazo[2,4], Julio C. Marín[1,5], Kyle R. Clem[6], Benjamin Pohl[7], Victoire Buffet[7,8], Vincent Favier[8], Tomás Carrasco-Escaff[2], and Bradford S. Barrett[9]

[1]Department of Meteorology, University of Valparaíso, Valparaíso, Chile.
[2]Center for Climate and Resilience Research CR2, Santiago, Chile.
[3]Center for Oceanographic Research COPAS COASTAL, University of Concepción, Concepción, Chile.
[4]Department of Geophysics, University of Chile, Santiago, Chile.
[5]Center for Atmospheric Studies and Climate Change (CEACC), University of Valparaíso, Valparaíso, Chile.
[6]School of Geography, Environment and Earth Sciences, Victoria University of Wellington, Wellington, New Zealand.
[7]Biogéosciences, CNRS/Université Bourgogne Europe, Dijon, France.
[8]Institut des Géosciences de l'Environnement, CNRS/Université Grenoble Alpes, Saint Martin d'Hères, France.
[9]Independent Scholar, Raleigh, NC, USA.

Correspondence to: Deniz Bozkurt (deniz.bozkurt@uv.cl)

Abstract. Atmospheric blocking is a key driver of persistent circulation anomalies and associated extreme events in the Southern Hemisphere, yet its characteristics around Antarctica remain poorly understood due to methodological diversity and the absence of a consolidated, long-term dataset. This study presents a new multi-method Antarctic atmospheric blocking dataset covering the period 1979-2024, derived from ERA5 reanalysis and constructed using multiple blocking detection approaches applied consistently across the Southern Hemisphere (25°S-90°S). The dataset integrates diagnostics based on 500 hPa geopotential height and vertically integrated potential vorticity within a unified framework for spatial filtering, event definition, and temporal tracking. It provides instantaneous blocking masks, spatiotemporally tracked event catalogs, time series, and aggregated climatologies that are directly comparable across methods. The results reveal only weak large-scale similarities in Antarctic blocking across detection approaches, mainly related to high latitude occurrence and seasonal modulation. In contrast, pronounced method dependent diversity is evident in blocking frequency, spatial extent, the number of detected blocking events, and persistence. Geopotential height-based methods identify a broader spectrum of anticyclonic flow regimes, including events extending into the Antarctic interior, whereas potential vorticity-based methods isolate fewer, more spatially confined events that emphasize dynamically coherent upper-level disturbances near the polar vortex. Event-based diagnostics further reveal systematic trade-offs between event frequency and duration, illustrating how different methodological choices preferentially capture either shorter-lived circulation anomalies or more persistent blocking structures. These contrasts arise from the diverse dynamical expressions of blocking at high southern latitudes, indicating that no single diagnostic fully captures Antarctic blocking behavior. Key uncertainties relate to threshold sensitivity, spatial filtering, and diagnostic formulation, which should be considered when interpreting blocking statistics and inter-method differences. By providing a consistent and openly accessible resource, this dataset allows direct intercomparison of blocking definitions, supports evaluation of climate models over Antarctica, and provides a foundation for future studies of blocking-related circulation variability and extreme events.

1 Introduction

Atmospheric blocking refers to a persistent, quasi-stationary anticyclonic anomaly in the mid-to-upper troposphere that interrupts the normal eastward progression of weather systems and diverts the prevailing westerly flow for periods of days to weeks (Rex, 1950; Woollings et al., 2018; AMS, 2026). It is a central feature of large-scale circulation that governs the persistence of weather patterns and often triggers extremes across the mid- and high latitudes (Woollings et al., 2018). Blocking over the Northern Hemisphere has been examined extensively for several decades, leading to a well-established understanding of its climatology, dynamics, and impacts (e.g., Dole, 1986; Carrera et al., 2004; Barriopedro et al. 2006; Barnes et al. 2014; Henderson et al., 2021). In contrast, comparatively few studies have focused on the Southern Hemisphere, where early work documented distinct blocking characteristics and preferred regions of occurrence, particularly over the South Pacific (Trenberth and Mo, 1985; Renwick, 1998; Renwick and Revell, 1999). Despite established links between Southern Hemisphere blocking and Antarctic circulation variability (Marshall and King, 1998), Antarctic blocking has rarely been examined using a coordinated, multi-method framework, limiting our ability to diagnose the circulation pathways that precede high-impact events (Sousa et al., 2021; Marín et al., 2022; Bozkurt et al., 2024).

The southern high latitudes are characterized by strong zonal flow and a unique combination of baroclinic and barotropic processes and atmosphere-ocean-ice interactions (e.g., Marshall et al., 2006; Fogt et al., 2012; Clem et al., 2022) that can shape the onset, maintenance, and decay of blocking systems. This dynamical environment challenges conventional approaches to blocking detection and has led to substantial methodological diversity in Antarctic and Southern Hemisphere studies. Existing approaches include gradient-reversal indices based on 500 hPa geopotential height (Pinheiro et al., 2019; Wang et al., 2024), a combined blocking–subtropical-ridge algorithm (Sousa et al., 2021), anomaly diagnostics based on 500 hPa geopotential height and potential vorticity (Pinheiro et al., 2019), and absolute-threshold methods implemented within objective feature-tracking frameworks (Ullrich et al., 2021). This diversity motivates a coordinated multi-method assessment of Antarctic blocking. As a result, long-term and method-consistent datasets for Antarctic blocking remain scarce, and this lack of coordinated information continues to restrict progress in Antarctic climate diagnostics and model evaluation.

This limitation has become more important as recent years have brought a series of extreme weather events across Antarctica. These include extreme warm intrusions (Turner et al. 2022; Wille et al. 2024a), record breaking surface temperatures (Bozkurt et al. 2018; Xu et al. 2021; Gorodetskaya et al. 2023), intense precipitation episodes (Gorodetskaya et al. 2014; Maclennan et al. 2023; Gilbert et al. 2025), and rapid sea ice loss and unprecedented melt conditions on the ice shelves and grounded ice sheet (Wille et al. 2022; Liang et al. 2023; Wille et al. 2025; Francis et al. 2025). Many of these events, often triggered by tropical convection, have been linked to atmospheric blocking that shapes atmospheric rivers, deep meridional moisture transport, and strong upper-level wave activity (e.g., Henderson et al., 2018; Rondanelli et al., 2019; Clem et al., 2021; Gorodetskaya et al., 2023; Baiman et al. 2024). In these situations, blocking directs moisture rich air toward the continent, sustains anomalous heat fluxes, and anchors circulation patterns that favor prolonged periods of high or low pressure (e.g., Pohl et al., 2021; Bozkurt et al., 2022; Wille et al., 2024a; Wang et al., 2024; Zhai et al., 2025) often in a preferred wavenumber-three pattern (Wang et al. 2019). In turn, blocking can be further amplified by atmospheric rivers through diabatic heating and latent heat release, reinforcing the persistence and intensity of extreme events (Wille et al. 2024b). In addition, blocking has been shown to influence surface mass balance, regional accumulation and melt, and the vulnerability of coastal ice shelves and sea ice to warm and moist air intrusions associated with persistent anomalous circulation patterns (Barrett et al., 2025; Wille et al., 2025). Despite these connections, a systematic and multi-method view of Antarctic blocking has been missing and this gap limits our ability to understand the dynamical pathways that lead to high impact events.

Many existing blocking studies rely on diagnostics developed for mid-latitude circulation regimes or focus on a single diagnostic field, most commonly 500 hPa geopotential height (Z500) (Woollings et al., 2018). Although blocking detected via these diagnostics is closely related to persistent anticyclonic circulation features, their applicability to Antarctic blocking remains uncertain, and systematic assessments for the Southern Hemisphere are still limited (Pepler, 2023). Circulation and height-based approaches have provided important insights, but they can miss features that are more directly tied to the dynamical structure of the polar vortex or to the vertical gradients that characterize the Antarctic troposphere and lower stratosphere. In recent years, studies have increasingly incorporated potential vorticity (PV) into blocking detection, as it captures coherent dynamical anomalies and helps distinguish barotropic wave activity from local circulation variability (e.g., Masato et al. 2013; Wachowicz et al., 2021; Polster and Wirth 2023; Hauser et al. 2024). The PV framework additionally supports decomposition of conservative and diabatic contributions to block onset and maintenance, offering mechanistic insight beyond detection alone (Hoskins et al., 1985; Hauser et al., 2024; Hauser et al. 2026). Pinheiro et al. (2019) offered advances in this direction by combining PV with geographically tailored thresholds and a clear procedure for persistence. Their work underscored the need for flexible detection strategies when describing Southern Hemisphere blocking, but a consolidated and openly accessible long-term dataset based on this framework has not been available.

The community has increasingly adopted objective feature detection and tracking frameworks to describe the life cycle of large-scale circulation systems. TempestExtremes is a widely used software framework that provides a consistent and reproducible approach for identifying and tracking features across gridded atmospheric fields (Ullrich et al. 2021). While it has been applied to a broad range of high-impact phenomena, TempestExtremes has not previously been used as a unified tracking framework for a multi-method Antarctic blocking dataset. By applying a streamlined implementation of its tracking capabilities, such dataset would enable a unified and consistent treatment of blocking events across detection methods.

Earlier work by Pinheiro et al. (2019) provided a dataset of Southern Hemisphere blocking characteristics derived from ERA-Interim for 1979 to 2018, based on multiple blocking diagnostics applied over the latitudinal band 25°S to 75°S within a unified threshold and tracking framework. In the present study, we extend this framework to cover a longer period (1979–2024) using the ERA5 reanalysis, which provides improved representation of Southern Hemisphere circulation relative to ERA-Interim through higher horizontal and temporal resolution, and an updated 4D-Var assimilation system that can better constrain upper-level wind, temperature, and potential vorticity fields, which can directly affect blocking detection (Hersbach et al., 2020; Ploeger et al., 2021; Hoffmann et al., 2022). We also expand the domain to 25°S–90°S for all blocking detection methods implemented in this dataset, except the gradient-based approach, which requires a 15° sampling distance and is therefore restricted to 25°S–75°S. Extending the remaining methods poleward is appropriate because blocking-like circulation anomalies have been documented at high Antarctic latitudes, including persistent anticyclonic structures embedded within or interacting with the polar circulation (Rex, 1950; Tang et al. 2026). Although such polar disturbances do not always satisfy classical mid-latitude definitions of blocking (Sousa et al. 2021), they can still modify circulation pathways, moisture transport, and surface conditions across Antarctica (e.g., Wang et al. 2024; Wille et al. 2025). Extending the domain over the full polar domain therefore allows these circulation anomalies to be represented consistently and provides a more complete description of flow regimes that influence the Antarctic climate system.

The resulting dataset combines recent advances in atmospheric blocking detection with the event tracking framework of TempestExtremes. It provides blocking masks, tracked events, and associated metadata derived from both Z500 and vertically integrated PV fields. All detection methods are applied consistently across the Southern Hemisphere over the study period and span from subtropical latitudes to Antarctica. The dataset incorporates four independent blocking diagnostics based on Z500 and three complementary diagnostics based on PV, following established formulations in the literature (e.g., Pinheiro et al., 2019). This design enables assessment of how diagnosed blocking depends on the chosen dynamical field and detection framework. Each event is tracked through time so that its duration, spatial footprint, and intensity can be analyzed in a fully reproducible way.

Three key features distinguish this dataset from other blocking datasets. First, it offers long-term, high temporal resolution coverage tailored to Antarctic circulation. Second, it brings together several blocking definitions that have previously been applied in isolation or limited case studies. Third, it uses a unified tracking framework that produces a harmonized catalog of blocking events with descriptors that are directly comparable across methods. Together, these features provide a robust reference for evaluating methodological sensitivity, assessing climate model performance, and examining the role of blocking in Antarctic weather and climate extremes.

The remainder of the paper is organized as follows. Section 2 describes the data sources and blocking detection methods. Section 3 outlines the dataset structure. Section 4 presents an overview of the resulting climatology and methodological differences, followed by a discussion of implications and potential applications. Section 5 describes where the dataset and code can be accessed. Section 6 summarizes the conclusions and outlook.

2 Data and Methodology

2.1 Reanalysis data

The dataset is constructed using atmospheric variables from the ERA5 global reanalysis (Hersbach et al., 2020) produced by the European Centre for Medium Range Weather Forecasts. ERA5 provides a physically consistent representation of the atmosphere at a horizontal spatial resolution of 0.25° × 0.25° and an hourly temporal resolution. ERA5 data were used at the native 0.25° × 0.25° horizontal resolution without regridding. We extracted Z500 and PV between 150 and 500 hPa for the Southern Hemisphere at 00, 06, 12 and 18 UTC from 1979–2024, corresponding to a vertical spacing of 25 hPa between 150 and 250 hPa and 50 hPa between 250 and 500 hPa. Although ERA5 provides hourly output, we use 6-hourly fields because these correspond to fully assimilated analysis time steps, whereas the intervening hourly fields are short-range forecasts and are therefore less observationally constrained. This choice also maintains consistency with Pinheiro et al. (2019) and is well suited to the analysis of atmospheric blocking, which evolves on timescales of days to weeks. This period offers 46 years of homogeneous data suitable for constructing long-term climatologies and robust event statistics. The 30-year period from 1991 to 2020 was selected as the climatological base for all methods that require a reference state. The Z500 level is widely used for blocking diagnostics because it captures the dominant large-scale structure of anticyclonic ridges. Vertically integrated PV provides a complementary dynamical perspective of PV gradients and upper-level wave breaking, which strongly influence blocking formation in the Southern Hemisphere (Dong and Colucci, 2005). The 150–500 hPa layer has been established as the region where PV anomalies most clearly reflect blocking dynamics (Pinheiro et al., 2019).

2.2 Preprocessing

2.2.1 Vertically integrated potential vorticity

PV was vertically integrated to obtain a dynamically coherent field that captures the large-scale upper-tropospheric and lower-stratospheric structures associated with blocking. The vertically integrated PV is defined as

$$\mathrm{PV}(\lambda, \phi, t) = \frac{1}{p_1 - p_2} \int_{p_2}^{p_1} \mathrm{PV}\,(\lambda, \phi, p, t)\, \mathrm{d}p \quad (1)$$

where p is the pressure coordinate, $\mathrm{d}p$ is the differential pressure increment used in the vertical integration, and λ, ϕ denote longitude and latitude on the regular ERA5 grid, respectively. Time is indicated by t and PV (λ, ϕ, p, t) is the PV value at that grid point and pressure level. The integration bounds follow the standard upper troposphere–lower stratosphere layer used in blocking diagnostics, where $p_1 = 150\,\mathrm{hPa}$ and $p_2 = 500\,\mathrm{hPa}$. Averaging over this layer filters out small-scale vertical variability and highlights the coherent PV anomalies associated with wave breaking and large-scale anticyclonic structures. This formulation follows the methodology used by Pinheiro et al. (2019), ensuring comparability between Z500 and PV blocking diagnostics.

2.2.2 Daily climatology and anomalies

A climatology for each calendar day was computed for the period 1991–2020 using the Climatology tool within TempestExtremes (Ullrich et al., 2021). The resulting fields were subsequently smoothed in time with a Fourier filter retaining the first five harmonics (*FourierFilter* function from TempestExtremes). This filtering suppresses short-term variability while preserving a smooth and physically realistic seasonal cycle. The same climatological procedure is used for both Z500 and PV, ensuring consistency across all detection methods.

Six-hourly anomalies were calculated by subtracting the smoothed daily climatology from the instantaneous ERA5 fields. The anomaly computation provides the foundation for the standard deviation–based and percentile–based blocking methods described later (see Table 1). Because short-lived sub-synoptic variability may obscure the slowly evolving signatures characteristic of blocking, each anomaly field was further smoothed using a 3-day running mean. This smoothing follows Pinheiro et al. (2019) and reduces the amplitude of short-lived anomalies, preventing transient ridges to satisfy the subsequent 3-day persistence criterion. This temporal smoothing reduces sensitivity to short-lived fluctuations without suppressing the persistent structures central to blocking identification.

2.2.3 Detrending of Z500 fields

A linear trend is removed from the Z500 time series independently at each grid point. The trend is estimated using an ordinary least squares regression applied to daily mean Z500 over the 1979–2024 period, with the regression accounting for the mean seasonal cycle through five annual harmonics. The detrended Z500 field is obtained by subtracting the fitted linear component (defined as the intercept plus a linear trend multiplied by time) from the original Z500 values at each time step, thereby preserving the seasonal and sub-seasonal variability. This detrending step is important because long-term increases in Z500 can otherwise introduce spurious temporal changes in anomaly-based diagnostics, leading to an artificial increase in the occurrence of extreme circulation states in some regions. For this reason, detrended Z500 fields are expected to be more appropriate for most applications. Nevertheless, the original Z500 fields are retained in the dataset to enable direct comparison and methodological evaluation.

2.3 Blocking Detection Methods

Blocking detection is performed using four methods applied to both Z500 and PV (the gradient method is only applied to Z500). After each detection step, the same minimum area threshold and temporal persistence criterion are applied to each method via TempestExtremes DetectBlobs and StitchBlobs, so that differences in blocking statistics across methods reflect the detection logic rather than post-processing inconsistencies. For threshold-based methods, smoothly varying climatological reference fields derived from 1991 to 2020 are used so that blocking detection reflects both the seasonal cycle and regional variability.

2.3.1 Gradient method

The gradient method (Z500-Grad) follows Pinheiro et al. (2019), which is itself a modification of the classical Tibaldi and Molteni (1990) algorithm. For each grid point located at longitude λ_0 and latitude ϕ_0, Z500 is sampled at two additional latitudes, 15° north and 15° south of the reference point. These latitudes are defined as

$$\phi_N = \phi_0 + 15^\circ, \quad \phi_S = \phi_0 - 15^\circ \tag{2}$$

Two meridional gradients are then computed at each grid point. The southward-directed gradient is given by

$$\text{GHGS}(\lambda_0, \phi_0) = \frac{Z_{500}(\lambda_0, \phi_0) - Z_{500}(\lambda_0, \phi_S)}{\phi_0 - \phi_S} \tag{3}$$

and the northward-directed gradient is given by

$$\text{GHGN}(\lambda_0, \phi_0) = \frac{Z_{500}(\lambda_0, \phi_N) - Z_{500}(\lambda_0, \phi_0)}{\phi_N - \phi_0} \tag{4}$$

Table 1. Overview of the blocking detection methods and their main characteristics. Methods are based on previously proposed diagnostics, including the gradient reversal of Tibaldi and Molteni (1990) as adapted by Pinheiro et al. (2019), the absolute threshold following Ullrich et al. (2021), and the standard deviation-based anomaly described by Pinheiro et al. (2019).

Feature	**Gradient Method (Z500-Grad)**	**Absolute Method (Z500-Abs / PV-Abs)**	**Standard deviation-based anomaly method (Z500-SD / PV-SD)**	**Percentile-based anomaly method (Z500-Perc / PV-Perc)**
Input Variables	Z500	Z500 PV (150–500hPa)	Z500 PV (150–500hPa)	Z500 PV (150–500hPa)
Climatology Base	Not used	Smoothed daily climatology (1991–2020)	Smoothed daily climatology (1991–2020)	Smoothed daily climatology (1991–2020)
Anomaly Calculation	Not used	Not used	Yes, relative to smoothed climatology	Yes, relative to smoothed climatology
Smoothing	None	Applied to the standard deviation threshold field	3-day moving average applied to anomalies	3-day moving average applied to anomalies

Threshold Type	Fixed meridional Z500 gradient reversal criteria: GHGN < 0 m °lat^{-1} and GHGS > 10 m °lat^{-1}	Smoothed daily climatology + max [100 m for Z500 or 1.1 PVU for PV, 1.5 × smoothed standard deviation]. The standard deviation is calculated from absolute values.	Max [100 m for Z500 or 1.1 PVU for PV, 1.5 × smoothed standard deviation of anomalies]. The standard deviation is calculated from smoothed anomalies.	Daily local 90th percentile of smoothed anomalies, calculated for each calendar day using a centered 15-day window (±7 days) pooled across 1991–2020.
Detection Method	Identify meridional gradient reversals in Z500	Identify grid cells exceeding the dynamic threshold	Identify grid cells exceeding the dynamic threshold	Identify grid cells exceeding the local percentile threshold for ≥ 3 consecutive days
Areal filter	Yes (minimum area 10^6 km²)			
Tracking Method	Spatially contiguous blocked regions are linked across successive time steps when they overlap by at least 1 grid cell. Events are retained only if they persist for at least 3 consecutive days.			

A grid cell is instantaneously blocked when both meridional gradients satisfy the following criteria (Tibaldi and Molteni, 1990; Pinheiro et al., 2019):

$$\mathrm{GHGN}(\lambda_0, \phi_0) < 0 \; \frac{\mathrm{m}}{°\mathrm{lat}} \tag{5}$$

and

$$\mathrm{GHGS}(\lambda_0, \phi_0) > 10 \; \frac{\mathrm{m}}{°\mathrm{lat}} \tag{6}$$

Sensitivity experiments varying the latitudinal sampling distance, the threshold applied to the southward meridional Z500 gradient (GHGS), and the minimum area filter are presented in supplementary material (Text S1.1 and Figs. S1 to S4). Over the Southern Ocean and Antarctic domain, the results are broadly insensitive to the latitudinal sampling distance (Fig. S2), whereas a discernible continental signal emerges only when both the GHGS threshold and the area filter are relaxed (Fig. S4) We retain the criterion GHGS > 10 m °lat^{-1} and a minimum area filter of 1.0 × 10^6 km^2 because these settings are consistent with Pinheiro et al. (2019) and preserve the role of Z500-Grad as a conservative flow-geometry baseline.

This pair of conditions indicates the presence of an anticyclonic ridge and represents a reversal of the climatological westerly flow. The method is applied over the latitude range 25°–75°S. Blocked grid cells are first identified using a Python script that computes the meridional geopotential height gradients and applies the blocking criteria. These blocked grid cells are then grouped into spatially contiguous regions using DetectBlobs, and regions that do not meet the minimum area requirement of 10^6 km² are discarded. The remaining regions are subsequently passed to StitchBlobs, which tracks their evolution through time. A blocking event is defined as any spatially coherent structure that persists for at least three days and exhibits spatial overlap of at least one grid cell between successive time steps.

2.3.2 Absolute threshold methods

The absolute-value methods identify blocking based on the magnitude of the raw Z500 (Z500-Abs) or PV (PV-Abs) field relative to a threshold that varies smoothly in space and time (Ullrich et al., 2021). In this method, a grid point at time t is classified as blocked when the actual field value equals or exceeds a threshold defined as the smoothed daily climatological mean plus a variability-dependent term. Formally,

$$X(\lambda, \phi, t) \geq \overline{X}_{\mathrm{clim}(\lambda,\phi,d(t))} + \max\left[\delta_{\mathrm{min}}, 1.5\, \sigma_{\mathrm{clim}(\lambda,\phi,d(t))}\right] \tag{7}$$

where X denotes Z500 or PV, $\overline{X}$ is the smoothed daily climatological mean, σ_{clim} is the smoothed daily standard deviation of the absolute field, δ_{min} is the fixed minimum threshold value, and $d(t)$ is the day of year corresponding to time step t. The fixed minimum value is 100 m for Z500 and 1.1 PVU for PV.

The climatological mean and standard deviation are computed over the 1991–2020 reference period. The climatological mean was smoothed using five harmonics in time. The climatological standard deviation was smoothed using two harmonics in longitude and five harmonics in time, following Pinheiro et al. (2019). Because the standard deviation is calculated from the absolute field, it includes variability associated with the full seasonal cycle. Blocking is defined where the field equals or exceeds its local threshold. Spatially contiguous blocked grid cells are then grouped using DetectBlobs, and the resulting regions are subsequently passed to StitchBlobs for temporal tracking and event identification, as described in Section 2.3.5.

2.3.3 Standard deviation-based anomaly methods

The standard deviation-based anomaly methods identify blocking from anomalies of Z500 (Z500-SD) and PV (PV-SD) that represent departures from the local climatological background rather than the absolute magnitude of the original field. These methods follow Pinheiro et al. (2019) with minor modifications and build on earlier anomaly-based blocking diagnostics applied to Z500 and PV, including those of Dole and Gordon (1983) and Schwierz et al. (2004). The key distinction from the absolute-threshold methods is that the blocking threshold is applied to the anomaly field, not to the raw Z500 or PV field. Anomalies are first defined relative to the smoothed daily climatological mean:

$$X'(\lambda, \phi, t) = X(\lambda, \phi, t) - \overline{X}_{\mathrm{clim}(\lambda,\phi,d(t))} \tag{8}$$

where X denotes Z500 or PV, X' is the corresponding anomaly, $\overline{X}_{clim}$ is the smoothed daily climatological mean, and $d(t)$ is the day of year corresponding to time step t. Blocking in this method is then defined from smoothed anomaly fields relative to the local climatology, with thresholds defined using the smoothed daily standard deviation of the anomalies (smoothed using two harmonics in latitude, two harmonics in longitude, and five harmonics in time, following Pinheiro et al. (2019)) over the 1991–2020 reference period, together with a fixed minimum value to avoid spurious detections in regions of weak variability.

In this framework, a grid point is classified as blocked when the smoothed anomaly equals or exceeds the local threshold:

$$X'(\lambda, \phi, t) \geq \max\left[\delta_{\min}, 1.5\, \sigma'_{\mathrm{clim}(\lambda,\phi,d(t))}\right] \tag{9}$$

Where X' is the smoothed anomaly field, σ'_{clim} is the smoothed daily standard deviation of the anomaly field, δ_{min} is the fixed minimum threshold value, equal to 100 m for Z500 or 1.1 PVU for PV (Pinheiro et al. 2019). Because the standard deviation is computed from anomalies rather than from the absolute field, it does not include variability associated with the full seasonal cycle, making the effective threshold distinct from that used in the absolute-threshold methods.

For Z500, anomalies are additionally adjusted using a latitude-dependent scaling following Pinheiro et al. (2019). This adjustment accounts for meridional differences in planetary wave geometry and ensures that anomaly magnitudes are dynamically comparable across latitude bands. This scaling is not applied to blocking defined using the percentile-based methods.

Sensitivity tests for the standard deviation-based anomaly methods are provided in supplementary material (Text S1.2 and Figs. S5 to S8). For Z500, the 50 m and 100 m thresholds give similar patterns, but 50 m produces more detections over the Antarctic interior, while 150 m misses substantial blocking over continental East Antarctica. For PV, 0.6 PVU produces widespread detections, whereas 1.6 PVU is overly restrictive. For the variability factor, a threshold of 1.0 standard deviation tends to pick up transient ridging and yields more frequent blocking detections, while a threshold of 2.0 standard deviations identifies fewer events. The fixed minimum threshold primarily controls detection over the Antarctic interior and other low-variability regions, whereas the variability-dependent term dominates over the Southern Ocean storm-track belt. Overall, the selected values of 100 m, 1.1 PVU, and 1.5 provide a physically reasonable balance between sensitivity and selectivity consistent with Pinheiro et al. (2019).

Blocked grid cells are grouped into spatially contiguous regions using DetectBlobs, which filters out grids that do not satisfy the minimum area requirement. The remaining regions are then passed to StitchBlobs, which applies the temporal persistence criterion and tracks the evolution of each blocking structure through time. A blocking event is defined using the same spatial coherence and temporal persistence criteria applied consistently across all detection methods.

2.3.4 Percentile-based anomaly methods

To complement existing anomaly-based blocking diagnostics, the percentile-based anomaly methods (Z500-Perc and PV-Perc) are developed in this study and identify blocking through sustained exceedances of locally extreme anomaly values. Thresholds are defined independently at each grid point from the empirical distribution of smoothed anomalies over the 1991–2020 reference period. For each calendar day, the local 90th-percentile threshold is calculated using anomalies within a centered 15-day running window (±7 days) pooled across all reference years. This window provides a sufficiently large sample for stable percentile estimates while preserving the gradual seasonal evolution of anomaly variability. Thus, detection is based on locally extreme values rather than on a fixed absolute magnitude.

For the percentile-based anomaly methods, grid points are first required to exceed the local percentile threshold for at least three consecutive days before spatial grouping. This persistence screening removes short-lived extremes prior to blob detection. Grid cells meeting this condition are then grouped into spatially contiguous regions using DetectBlobs, with regions failing to meet the minimum instantaneous area requirement discarded. The remaining regions are passed to StitchBlobs for event tracking, ensuring that percentile-based blocking events satisfy the same persistence criteria applied across all detection methods while retaining sensitivity to locally extreme circulation anomalies.

2.3.5 Event definition, areal filtering, and tracking

The event definition and tracking procedure is applied uniformly to all blocking detection methods described above. All detection methods produce instantaneous binary masks that identify grid points satisfying the respective blocking criteria. These masks are processed using the DetectBlobs and StitchBlobs algorithms implemented in TempestExtremes to construct spatially coherent features and analyze their temporal evolution. At each time step, DetectBlobs groups adjacent blocked grid cells into contiguous regions and applies a minimum areal constraint. The spatial filtering removes small-scale features associated with transient or locally confined anomalies, ensuring that only synoptic-scale circulation structures characteristic of atmospheric blocking are retained. Following Pinheiro et al. (2019), a common minimum area requirement of 1.0×10^6 km^2 is imposed for all methods, and regions that do not meet this requirement are discarded prior to event tracking. Although this threshold may suppress smaller-scale blocking-like features, particularly over the Antarctic interior, it is retained to ensure that inter-method differences arise primarily from the detection criteria rather than from method-specific post-processing. Because Z500, PV, and gradient-based fields have different spatial coherence, the common filter can contribute to differences in event counts among methods. Sensitivity tests for the area filter are provided in supplementary materials (Text S1.1 and S1.3; Figs S1, S3, S4, S9, and S10) and show that the principal spatial patterns are robust to reducing the filter to 0.5×10^6 km^2.

After applying the areal constraint, StitchBlobs links spatially coherent regions across consecutive time steps when they overlap by at least one grid cell. Because grid-cell area decreases toward the pole, a one-grid-cell overlap represents a smaller physical area at high latitudes than at lower latitudes. The overlap criterion is therefore less restrictive near the pole and may affect absolute persistence estimates at very high latitudes. This limitation is common to all methods and does not affect their relative comparison. Sensitivity tests varying the minimum overlap fraction in StitchBlobs show no significant effect on blocking-frequency patterns for the tested Z500-Grad, Z500-SD, and PV-SD methods (Figs. S11-S13). A blocking event is defined as a spatially coherent structure that persists for at least three consecutive days under the tracking procedure. This three-day requirement, referred to as the temporal persistence criterion, is applied uniformly across all blocking methods so that differences among methods reflect their underlying detection logic rather than inconsistencies in event construction. While earlier studies of persistent height anomalies employed longer thresholds (e.g., five days in Dole and Gordon, 1983), the shorter criterion adopted here accounts for the faster mean flow, stronger jet, and interactions with the polar vortex that can characterize blocking events in the Southern Hemisphere and Antarctic circulation.

The complete blocking workflow, from ERA5 input fields through preprocessing, detection and event tracking, is summarized schematically in Fig. 1. An illustrative example of a blocking event detected and tracked using the Z500 percentile-based anomaly method is shown in Fig. 2.

3 Dataset Structure and Contents

The Antarctic blocking dataset is organized to provide users with a uniform and transparent structure across all detection methods and variables. Each method produces a complete set of data products that describe instantaneous blocking conditions, event-level connectivity, and long-term statistics. The dataset is arranged so that users can compare methods directly, reproduce analyzes, and incorporate blocking information into studies of circulation variability and Antarctic climate processes.

Each blocking detection method is distributed in a dedicated directory named according to the variable and methodology employed: absolute threshold method (Z500-Abs, PV-Abs), gradient method (Z500-Grad), percentile-based anomaly method (Z500-Perc, PV-Perc), and standard deviation-based anomaly method (Z500-SD, PV-SD). Within each directory, the data are grouped into four subfolders, *blocking*, *blocking_id*, *clim*, and *time_series*, which collectively provide information at instantaneous, event, climatological, and temporally aggregated (e.g., seasonal or annual) scales (Fig. 3). All files follow consistent naming conventions, include full metadata, and adhere to NetCDF-CF standards.

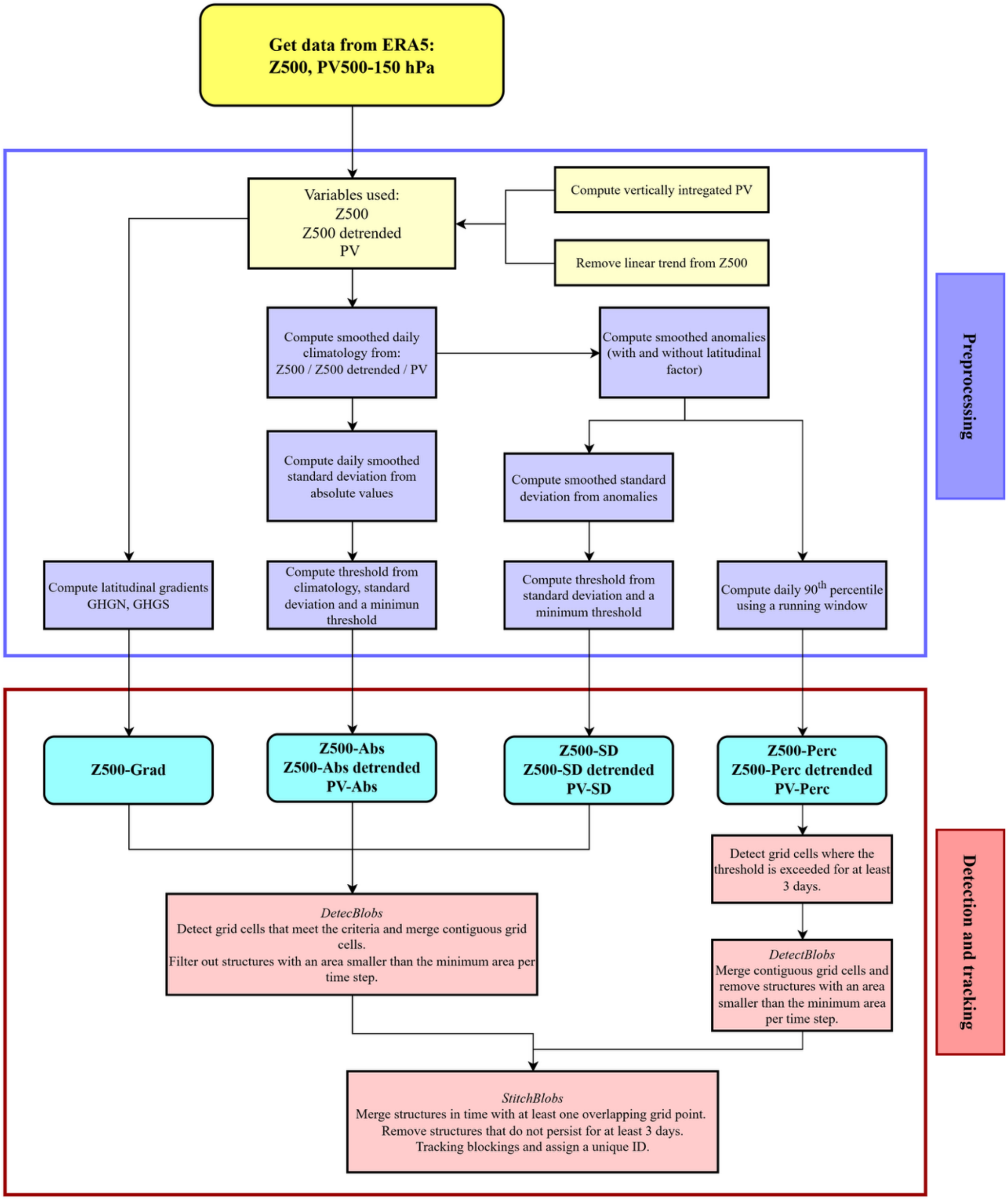

Figure 1: Schematic overview of the data processing and blocking detection workflow. ERA5 Z500 and pressure-level potential vorticity are preprocessed through vertical integration, detrending, climatology and anomaly calculations, and threshold construction. Multiple blocking detection methods are then applied, followed by a unified areal filtering and event tracking procedure using DetectBlobs and StitchBlobs from TempestExtremes.

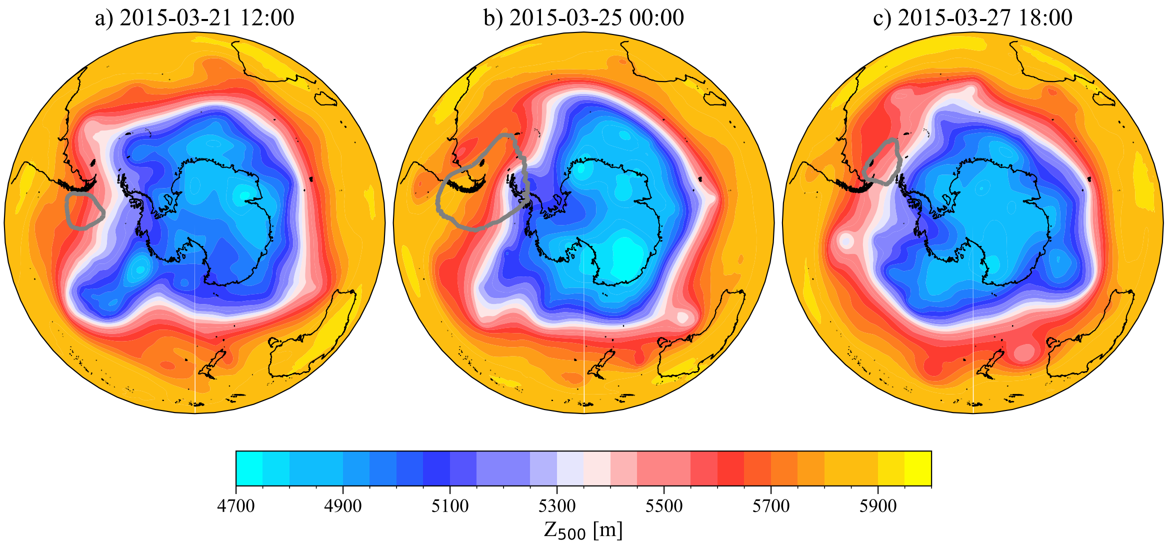

Figure 2: Illustrative example of a blocking event detected using the Z500 percentile-based anomaly method in March 2015. Shaded colors show the absolute geopotential height at 500 hPa (Z500), while gray contours indicate the spatial extent of the detected blocking region. Blocking identification in the percentile-based methodology is based on locally extreme and persistent anomalies relative to the climatology, rather than on absolute height magnitude. Panels illustrate the temporal evolution of the event at selected time steps during its lifetime.

3.1 Instantaneous blocking fields

The *blocking* directory contains the 6-hourly instantaneous blocking masks for the 1979–2024 period. These fields are the direct output of the detection methods described in Section 2. Each file consists of a binary grid where a value of one indicates blocked flow and a value of zero indicates unblocked flow. The fields preserve the native 0.25° × 0.25° ERA5 grid and allow users to examine the spatial and temporal evolution of blocking episodes. These data are intended for diagnostic analyzes, comparison of blocking structures across methods, and integration with other atmospheric variables.

3.2 Event identification and tracking

The *blocking_id* directory contains labeled blocking fields generated using the StitchBlobs tracking algorithm. Each blocked grid cell is assigned an event identifier (ID), whereas non-blocked grid cells are assigned a value of zero. Tracking is based on spatial overlap between blocking regions at consecutive time steps. In this dataset, regions are considered temporally connected when they overlap by at least one grid cell. StitchBlobs does not impose a one-to-one correspondence between structures. Thus, blocking regions that split from a parent region or merge into a single region can retain a common ID through the overlap-based stitching procedure. The dataset does not include a separate catalog of merging and splitting events, but these interactions can be reconstructed from the temporal evolution of the labeled fields. The fields support event-based diagnostics such as duration, spatial extent, displacement, intensity, and the evolution of blocking structures.

3.3 Aggregated time series

The *time_series* directory provides temporally aggregated time series of blocking metrics for the Southern Hemisphere. These time series describe the temporal evolution of blocking characteristics evaluated over fixed aggregation intervals, including monthly, seasonal, and annual periods, and are derived consistently for each blocking detection method. Three variables are provided: blocking frequency, blocking intensity, and blocking persistence.

a)

```
Dataset Root
│
├── Z500-Abs/
│     ├── blocking/
│     ├── blocking_id/
│     ├── clim/
│     └── time_series/
│
├── Z500-Grad/
│     ├── blocking/
│     ├── blocking_id/
│     ├── clim/
│     └── time_series/
│
├── Z500-Perc/
│     ├── blocking/
│     ├── blocking_id/
│     ├── clim/
│     └── time_series/
│
├── Z500-SD/
│     ├── blocking/
│     ├── blocking_id/
│     ├── clim/
│     └── time_series/
│
└── Z500-Abs_detrend, Z500-Perc_detrend, Z500-SD_detrend,
      PV-Abs, PV-Perc, PV-SD
      (each with the same four subfolders)
```

b)

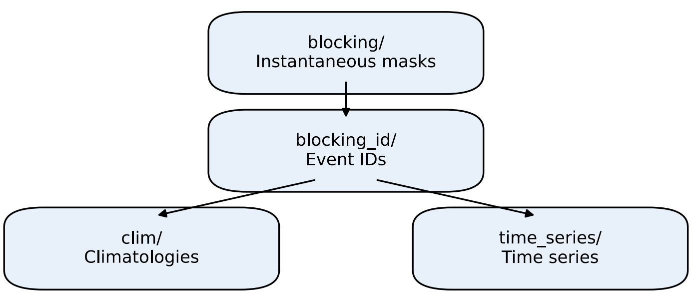

Figure 3: a) Directory structure of the Antarctic blocking dataset. Each blocking detection method (e.g., Z500-Abs, Z500-Grad, Z500-Perc, Z500-SD, and their detrended variants, as well as PV-Abs, PV-Perc, and PV-SD) is stored in a dedicated folder containing four subdirectories: blocking, blocking_id (fields labeled with unique blocking event identifiers), clim (annual, seasonal, and monthly climatologies), and time_series (aggregated Southern Hemisphere time series). All methods follow this identical structure to ensure consistency and comparability across variables and detection approaches. b) Schematic representation of the data flow. Blocking masks are used to identify and track blocking events whose unique event identifiers are stored in the blocking_id fields and subsequently support the generation of climatologies and aggregated time series.

Blocking frequency represents the proportion of time steps classified as blocked relative to the total number of time steps within each aggregation period. Blocking intensity reflects the characteristic magnitude of the underlying field during blocked conditions and is calculated as the mean value of the relevant variable over all blocked time steps within each aggregation period. For the Z500-Grad method, blocking intensity is defined as the mean absolute value of the geopotential height gradients GHGN and GHGS during blocked conditions. Blocking persistence represents the mean duration of blocking events affecting each grid cell and is calculated as the total blocked time divided by the number of blocking events passing through that grid cell within the aggregation period. Blocking intensity and persistence are undefined where no blocking events occur.

These aggregated time series enable analyzes of temporal variability, long-term behavior, and potential trends in blocking characteristics. Because the time series are aggregated consistently for all methods, they allow direct comparison of interannual and decadal blocking variability across detection approaches and between the Z500- and PV-based formulations.

3.4 Climatological blocking fields

The *clim* directory contains long-term climatological fields derived from the aggregated time series over the 1979–2024 period. These climatologies summarize the mean characteristics of blocking and are provided at annual, seasonal, and monthly temporal resolutions for each detection method. Each timescale includes three variables: blocking frequency, blocking intensity, and blocking persistence.

The climatological blocking frequency describes the average fraction of time blocked at each grid cell. The climatological number of blocking events represents the mean occurrence of distinct blocking events affecting each location. Climatological blocking intensity and persistence characterize the typical magnitude and duration of blocking events at each grid cell, based on the definitions used in the time series products.

These climatological fields provide a method-consistent summary of blocking behavior and serve as a reference for assessing large-scale circulation variability and for evaluating how atmospheric and climate models reproduce key aspects of blocking, including its spatial distribution, seasonal cycle, event frequency, and characteristic duration.

3.5 Consistency, metadata, and reproducibility

All files adhere to standardized naming conventions that encode the variable, detection method, temporal scale and the Southern Hemisphere domain. Metadata include units, coordinate definitions, calendar information, and method identifiers to ensure long-term reproducibility and clarity. The consistent internal structure across detection methods ensures that users can substitute one method for another without requiring adjustments to data handling workflows. This design enables comparative analyzes of blocking sensitivity across methods, facilitates the use of the dataset in modeling studies, and supports integration with complementary Antarctic climate datasets.

The dataset organization also ensures compatibility with common scientific workflows. The 6-hourly masks allow high-resolution diagnostics; the event ID fields provide a foundation for object-based analysis; the climatological fields permit long-term spatial comparison; and the time series summarize domain-integrated blocking behavior. Together, these components provide a comprehensive and flexible dataset supporting Antarctic circulation and extreme-event research.

4 Results and Discussion

This section presents several characteristics of Antarctic atmospheric blocking as derived from the different detection methodologies included in the dataset. Results are organized to first describe the spatial distribution of blocking frequency on annual and seasonal time scales, followed by an analysis of event-based characteristics including frequency, persistence, and intensity. Finally, selected case studies are used to illustrate similarities and divergences among methods at the synoptic scale. Throughout this section, emphasis is placed on identifying robust signals that emerge consistently across methods, as well as on clarifying methodological sensitivities and sources of uncertainty.

4.1 Annual climatology of blocking frequency

The annual mean blocking frequency derived from the different detection methods is shown in Fig. 4. The methodological diversity among approaches leads to substantial differences in the large-scale spatial patterns of blocking across the Southern Hemisphere. Nevertheless, most methods identify some common broad features, with the notable exception of the Z500-Grad approach. Several methods indicate that blocking activity is preferentially located at mid- to high-southern latitudes, while enhanced frequencies form circumpolar bands in a subset of methods, particularly Z500-SD and PV-SD. Other approaches show blocking maxima centered over the Antarctic continent or a more spatially homogeneous distribution, as in the Z500-Perc and PV-Perc methods, respectively.

The Z500-Grad method depicts a narrow and zonally continuous band of blocking confined primarily to the mid-latitudes of the Southern Ocean (Fig. 4a). Blocking identified by this method is concentrated roughly between 40°S and 60°S, reflecting its sensitivity to meridional reversals of the mid-latitude westerlies rather than broad anticyclonic anomalies extending into the polar cap. As a result, blocking frequencies over Antarctica itself are relatively low, with the climatological signal strongest in the mid-latitude regions near southern Africa and Australia. Within this circumpolar band, clear longitudinal asymmetries are evident, with relatively higher blocking frequencies over the South Pacific sector and weaker occurrence over the South Atlantic and Indian Ocean sectors. This pattern highlights the close association of the gradient method with Southern Ocean storm track and the mean flow, rather than with high-latitude continental blocking structures. These low Antarctic frequencies reflect the specific flow-geometry criterion targeted by Z500-Grad, namely reversal of the meridional Z500 gradient, rather than broad persistent anticyclonic anomalies. The contrast with the threshold-based methods is therefore an informative result of the dataset, indicating how diagnosed Antarctic blocking depends on the underlying detection concept. Z500-Grad is retained as a conservative flow-geometry baseline and to enable direct comparison with published studies using gradient-based diagnostics (e.g., Pinheiro et al., 2019).

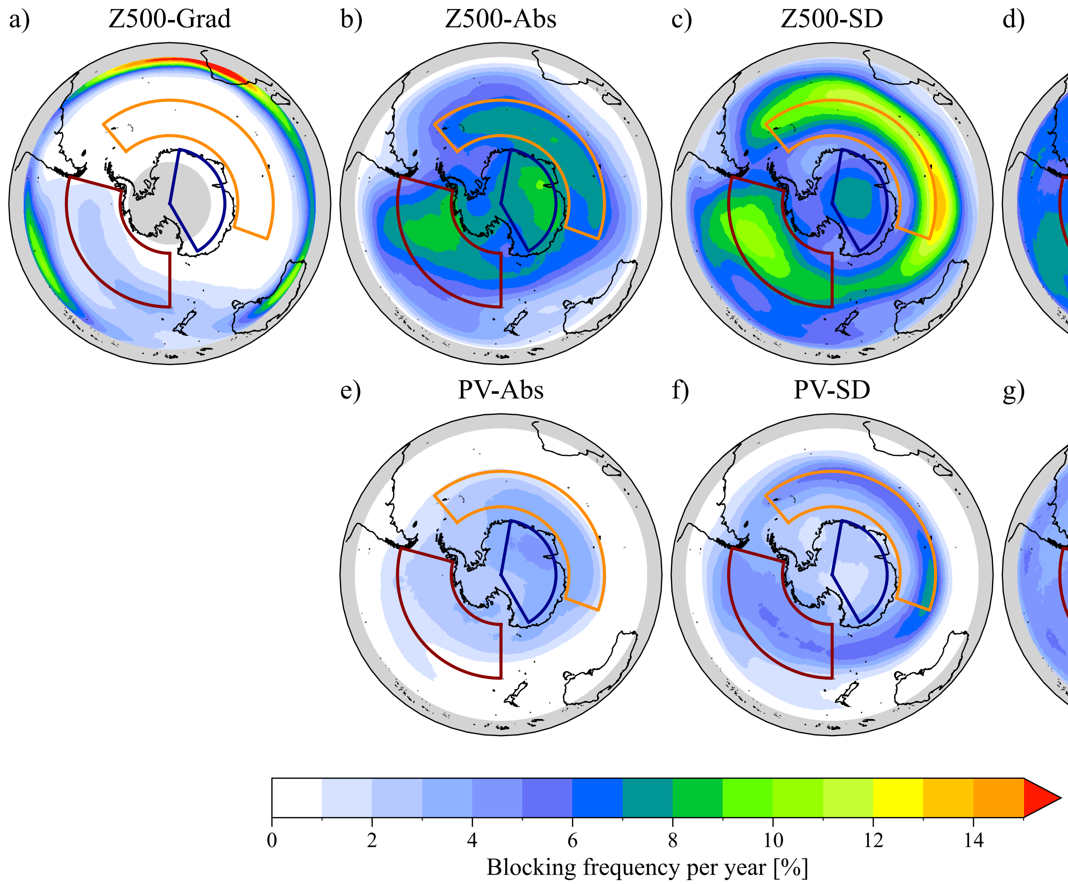

Figure 4: Annual climatology of Antarctic atmospheric blocking frequency expressed as the percentage of blocked days per year for each detection method. Panels show results for Z500 based methods a) Z500 gradient, b) Z500 absolute threshold, c) Z500 standard deviation-based anomaly, d) Z500 percentile-based anomaly, and PV based methods e) PV absolute threshold, f) PV standard deviation-based anomaly, and g) PV percentile-based anomaly. The polygons denote the regional domains used for the area averaged statistics in Figure 6. Regions shown in gray correspond to latitudes where blocking detection is not applied (north of 25°S for all methods and south of 75°S for Z500-Grad).

In contrast with the gradient method, the threshold-based Z500 methods (Z500-Abs, Z500-SD, and Z500-Perc) suggest broader and more spatially extensive blocking patterns, with clear differences among the individual formulations. The Z500-Abs method identifies widespread blocking across much of the Antarctic continent and the surrounding Southern Ocean, with enhanced frequencies extending from the coastal margins into the interior (Fig. 4b). Local maxima are evident over East Antarctica and in the Amundsen Sea sectors, highlighting the sensitivity of this method to large amplitude geopotential height anomalies that affect both continental and oceanic regions. The Z500-SD method exhibits the strongest annular structure among the Z500-based methods (Fig. 4c). High blocking frequencies form a near continuous ring around Antarctica, with maxima concentrated over the Southern Ocean and a minimum over the Drake Passage. This pattern reflects the influence of climatological variability on the anomaly-based threshold, which preferentially highlights regions of large geopotential height fluctuations associated with the polar front and storm track. Blocking occurrence over the continental interior is less frequent in the threshold methods than in the Z500-Abs method. The Z500-Perc method produces a relatively uniform background blocking frequency over the Southern Ocean with a pronounced and spatially extensive enhancement over East Antarctica (Fig. 4d). Blocking over the continental interior is more widespread than in both the Z500-SD and Z500-Abs methods, consistent with the locally defined nature of the percentile threshold, which reduces the dominance of regions with inherently large variability and enhances sensitivity to persistent continental anomalies.

The PV-based methods exhibit lower blocking frequencies and weaker spatial contrasts than the Z500-based methods, reflecting both methodological and dynamical differences. Methodologically, the sensitivity analysis shows that lowering the fixed PV minimum threshold from 1.1 to 0.6 PVU substantially increases detection frequency (Fig. S6). Dynamically, vertically integrated PV anomalies associated with blocking are generally more spatially compact than Z500 anomalies because the vertical integration retains only coherent upper-tropospheric features (Schwierz et al., 2004; Hauser et al. 2024; Hauser et al. 2026). A systematically lower PV blocking frequency relative to Z500 under comparable settings has also been reported for the Southern Hemisphere by Pinheiro et al. (2019). The PV-Abs and PV-SD methods show similar spatial patterns, with greater blocking frequencies aligned along the outer edge of the polar vortex, particularly in the mid- to high-latitude Southern Ocean (Fig. 4e, f). In contrast, the PV-Perc method produces the most spatially homogeneous distribution among the PV-based approaches, with relatively uniform blocking frequencies across the polar cap and weaker longitudinal structure (Fig. 4g). Blocking over the Antarctic interior is present but more attenuated than in the Z500-based methods.

4.2 Seasonality of blocking frequency

The seasonal modulation of blocking frequency for the Z500- and PV-based methods is shown in Fig. 5 and reveals a method-dependent seasonal structure rather than a uniform summer-winter contrast (Fig. 5).

During December-January-February (DJF), the Z500-based methods display marked differences in the spatial organization of blocking rather than a uniform pattern. The Z500-Grad method identifies limited blocking over Antarctica itself, with activity largely confined to the mid-latitudes (Fig. 5a), whereas Z500-Abs and Z500-Perc indicate more frequent blocking over coastal and interior Antarctic regions (Figs. 5b, d). The Z500-SD method emphasizes a circumpolar ring of highest blocking activity over the Southern Ocean, with comparatively weaker signals over the continental interior (Fig. 5c).

In June-July-August (JJA), the spatial distribution of blocking over high latitudes changes markedly. The Z500-Grad method shows localized enhancements in blocking over the Amundsen and Bellingshausen Sea sectors, where the mid-latitude jet weakens and becomes less zonally continuous over the South Pacific (Trenberth and Mo, 1985; Renwick and Revell, 1999) (Fig. 5e). This pattern suggests that regional ridging can influence the polar circulation during winter, preferentially emerging in regions where the westerlies and associated storm track are less dominant. The Z500-SD method shows relatively enhanced blocking over parts of the Antarctic continent and adjacent seas, indicating a redistribution of blocking activity toward the polar cap (Fig. 5g). The Z500-Abs and Z500-Perc methods similarly show winter blocking concentrated in the high latitudes, particularly in regions where large-scale anticyclonic height anomalies project onto the polar circulation, although these occurrences are relatively fewer and more spatially confined in JJA compared to DJF (Figs. 5f, h).

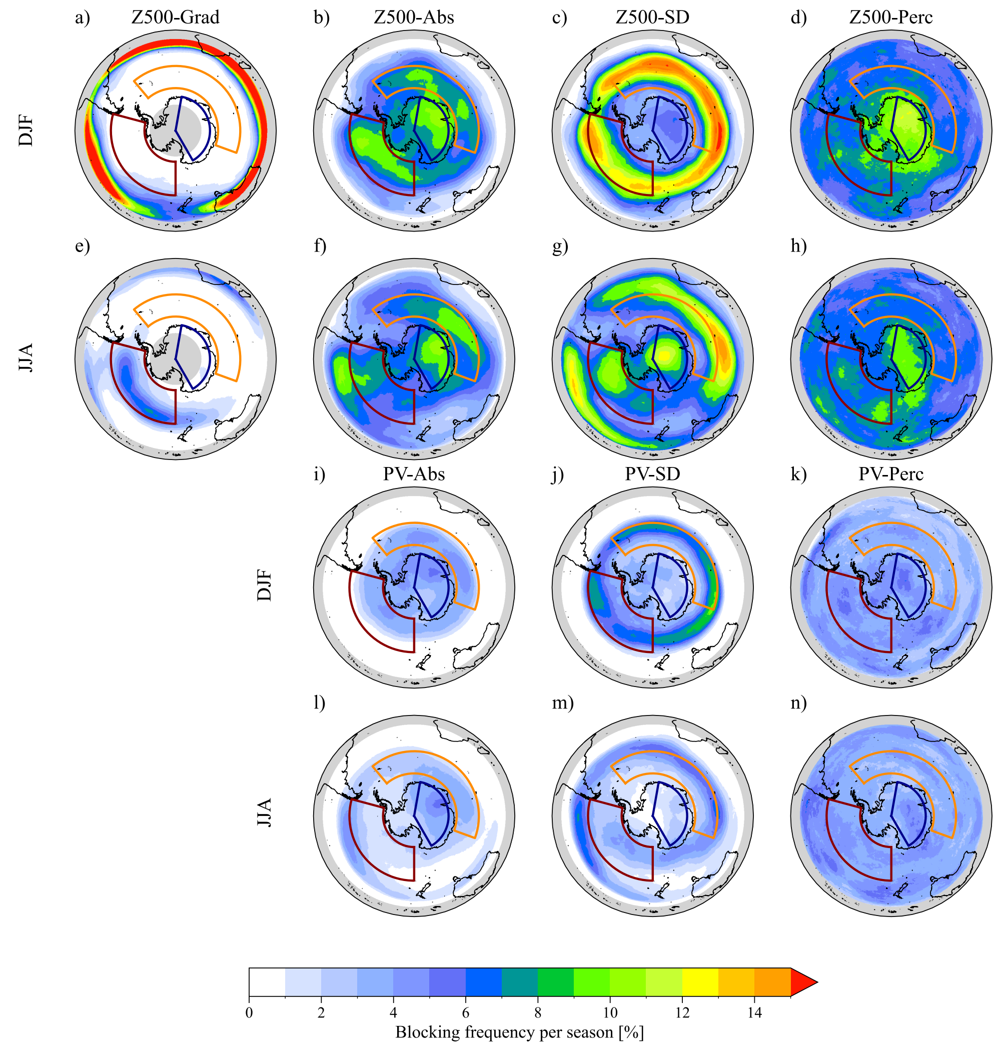

Figure 5: Seasonal climatology of Antarctic atmospheric blocking frequency expressed as the percentage of blocked days per season for Z500- and PV-based methods. Panels a) to d) show austral summer (December-January-February) for the Z500 gradient, Z500 absolute threshold, Z500 standard deviation-based anomaly, and Z500 percentile-based anomaly methods, respectively. Panels e) to h) show the results for austral winter (June-July-August). Panels i) to k) and l) to n) show the austral summer and winter climatologies, respectively, for the PV absolute threshold, PV standard deviation-based anomaly, and PV percentile-based anomaly

methods. The polygons denote the regional domains used for the area averaged statistics in Figure 6. Regions shown in gray correspond to latitudes where blocking detection is not applied (north of 25°S for all methods and south of 75°S for Z500-Grad).

The PV-based methods display a broadly consistent seasonal modulation but with systematically lower blocking frequencies and a more muted spatial structure. In DJF, the PV-Abs and PV-Perc methods show weak and diffuse blocking activity over the Antarctic region, with limited organization over the Southern Ocean and little penetration into the continental interior (Figs. 5i, k). In contrast, the PV-SD method highlights a clearer circumpolar structure, with enhanced blocking frequency over the Southern Ocean storm track (Fig. 5j). During JJA, blocking detected via PV-based methods remains relatively weak overall, with modest increases over the Southern Ocean and localized enhancements near the Antarctic margin, but without the pronounced continental signals seen in blocking detected by the Z500-based methods (Figs. 5l–n). This reduced spatial contrast reflects the greater dynamical constraint of vertically integrated PV and its sensitivity to large scale, vertically coherent circulation anomalies.

To complement the spatial climatologies, we selected three broad Antarctic regions: West Antarctica (75–180°W, 50–72°S), East Antarctica (40°W–110°E, 50–65°S), and continental East Antarctica (10–150°E, 70–90°S), depicted by the colored polygons in Fig. 5. Figure 6 summarizes blocking frequency averaged over each domain, with temporal mean and standard deviation of area-weighted regional averages derived from annual and seasonal climatologies.

The regional averages confirm the methodological contrasts apparent in the spatial climatologies. The Z500-Abs, Z500-SD, and Z500-Perc methods yield the highest blocking frequencies across all three regions, with annual values generally between approximately 6% and 10%. In contrast, Z500-Grad indicates frequent blocking mainly in West Antarctica, particularly in JJA, while yielding near-zero frequencies over East Antarctica and continental East Antarctica. This low continental signal should be interpreted in light of the sensitivity tests: enhanced continental detection emerges only when both the GHGS threshold and area filter are relaxed (Text S1.1; Fig. S4), whereas the retained configuration provides a conservative flow-geometry baseline. The PV-based methods generally produce lower frequencies and weaker seasonal contrasts, consistent with their sensitivity to vertically coherent, large-scale circulation anomalies.

The largest temporal variability occurs for DJF frequencies over continental East Antarctica, particularly for the Z500-based methods, indicating substantial temporal variability in the regional mean blocking frequency. Seasonal differences are most evident in West Antarctica and East Antarctica, whereas continental East Antarctica shows weaker mean seasonal contrasts but considerable temporal variability.

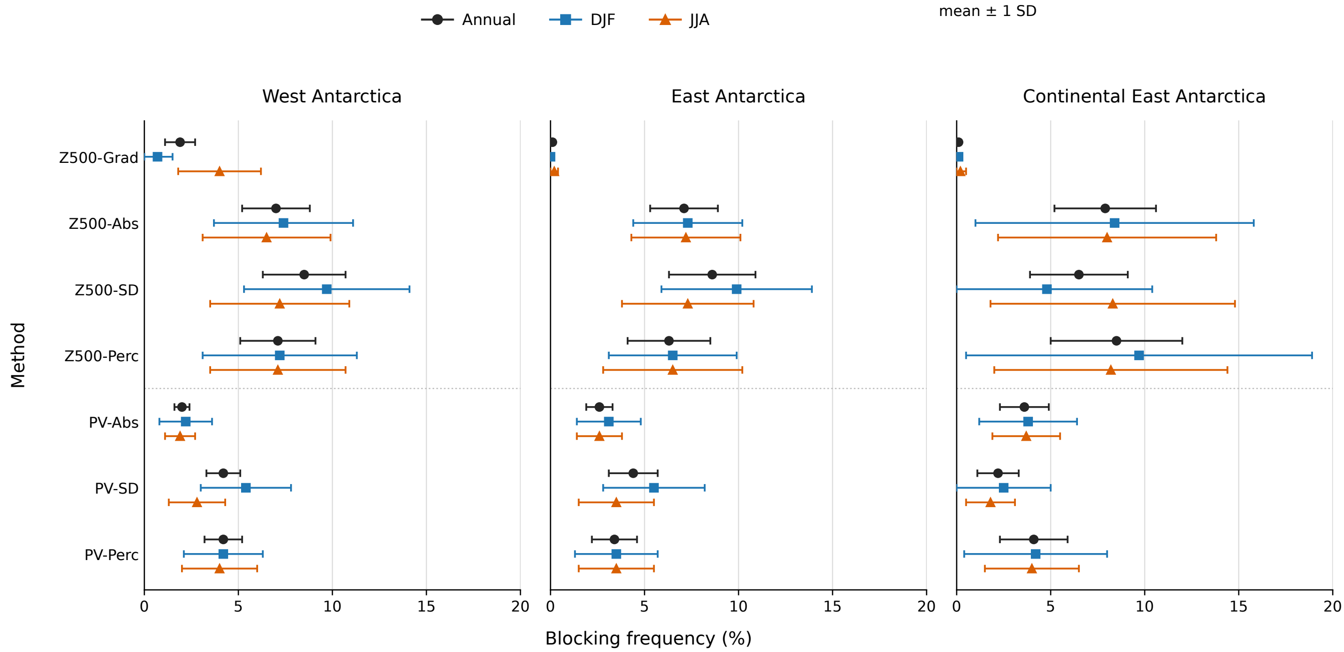

Figure 6: Annual and seasonal mean Antarctic blocking frequency (%) for seven detection methods across West Antarctica (75–180°W, 50–72°S), East Antarctica (40°W–110°E, 50–65°S), and continental East Antarctica (10–150°E, 70–90°S; regions shown in Fig. 5). Symbols show the mean area-weighted regional percentage of blocked days, and horizontal bars indicate ±1 temporal standard deviation. Black circles denote annual values, blue squares austral summer (DJF), and orange triangles austral winter (JJA). The horizontal dashed line separates the Z500- and PV-based methods.

4.3 Methodological uncertainty in blocking frequency

The results presented in Sections 4.1 and 4.2 show that the frequency and spatial variability of Antarctic blocking are fundamentally shaped by methodological choices in both variable and threshold selection. Blocking based on Z500 captures a broad spectrum of anticyclonic regimes, including high-amplitude anomalies projecting into the polar cap, consistent with their sensitivity to persistent, quasi-stationary highs (Renwick, 1998; Grotjahn et al., 2016). These methods are effective at identifying regions of weakened or reversed zonal flow, but may conflate true dynamical blocking with other persistent positive anomalies (Davini et al., 2012). In contrast, blocking based on PV identifies a more restricted subset of events, emphasizing large-scale, coherent wave breaking and vortex interactions over localized amplitude extremes, resulting in lower, more zonally constrained frequencies (Masato et al., 2013; Polster and Wirth, 2023). This reflects a stricter focus on anomalies with direct dynamical connection to the hemispheric potential vorticity gradient.

The seasonal cycle further illustrates these diagnostic sensitivities observed at the annual scale. The observed redistribution in blocking from summer to winter reflects differing responses to the strengthening and increased zonal symmetry of the polar vortex (Nakamura and Huang, 2018), as well as intraseasonal modulation of Southern Hemisphere wave activity that can favor clustered blocking during specific circulation states (Henderson et al., 2018; Liu and Wang, 2024). Potential mechanisms relevant to winter high-latitude blocking include regional ridge amplification driven by horizontal wave propagation and anticyclonic vorticity advection linked to Rossby wave activity, as documented in recent studies of extreme Antarctic circulation anomalies, as well as interactions with the stratospheric circulation that can reinforce or prolong blocking events (e.g., Gorodetskaya et al. 2023; Lim et al. 2026; Tang et al. 2026).

To quantify the relative importance of the blocking metric and diagnostic variable, we calculated two uncertainty measures from the 1979–2024 blocking-frequency time series at each grid point. Metric uncertainty, σ_{metric}, was calculated as the time-mean standard deviation across the three methods shared by both variables (absolute threshold, standard deviation-based anomaly, and percentile-based anomaly), separately for Z500 and PV; the two resulting values were then averaged. Variable uncertainty, $\sigma_{variable}$, was calculated as the time-mean standard deviation between Z500- and PV-based blocking frequencies, separately for each of the three shared methods; these values were then averaged across methods. The gradient method was excluded because it has no PV counterpart. The dominance ratio, R, was obtained by dividing σ_{metric} by $\sigma_{variable}$. Values of R above one indicate that uncertainty is dominated by the choice of blocking metric, whereas values below one indicate that it is dominated by the choice of diagnostic variable (Fig. 7).

The resulting dominance ratio shows that, over most of Antarctica and across all seasons, uncertainty is primarily controlled by whether blocking is diagnosed from Z500 or PV, rather than by the specific technique used to quantify blocking. This dominance of variable choice is particularly evident over the Antarctic interior and large sectors of the surrounding Southern Ocean, where Z500- and PV-based diagnostics yield systematically different blocking frequencies. In contrast, localized regions along the Antarctic coastal margins and parts of the storm-track belt exhibit dominance ratios closer to unity, indicating a more comparable influence of metric and variable choices.

These systematic contrasts confirm that methodological differences are not merely inconsistencies but instead reveal complementary physical phenomena. The Z500-based methods provide a comprehensive view of persistent anticyclonic conditions, while the PV-based methods isolate dynamically coherent upper-tropospheric disruptions. A multi-metric framework is therefore essential for a complete understanding of persistent high-latitude circulation regimes, their seasonal evolution, and their impacts on surface climate and sea ice.

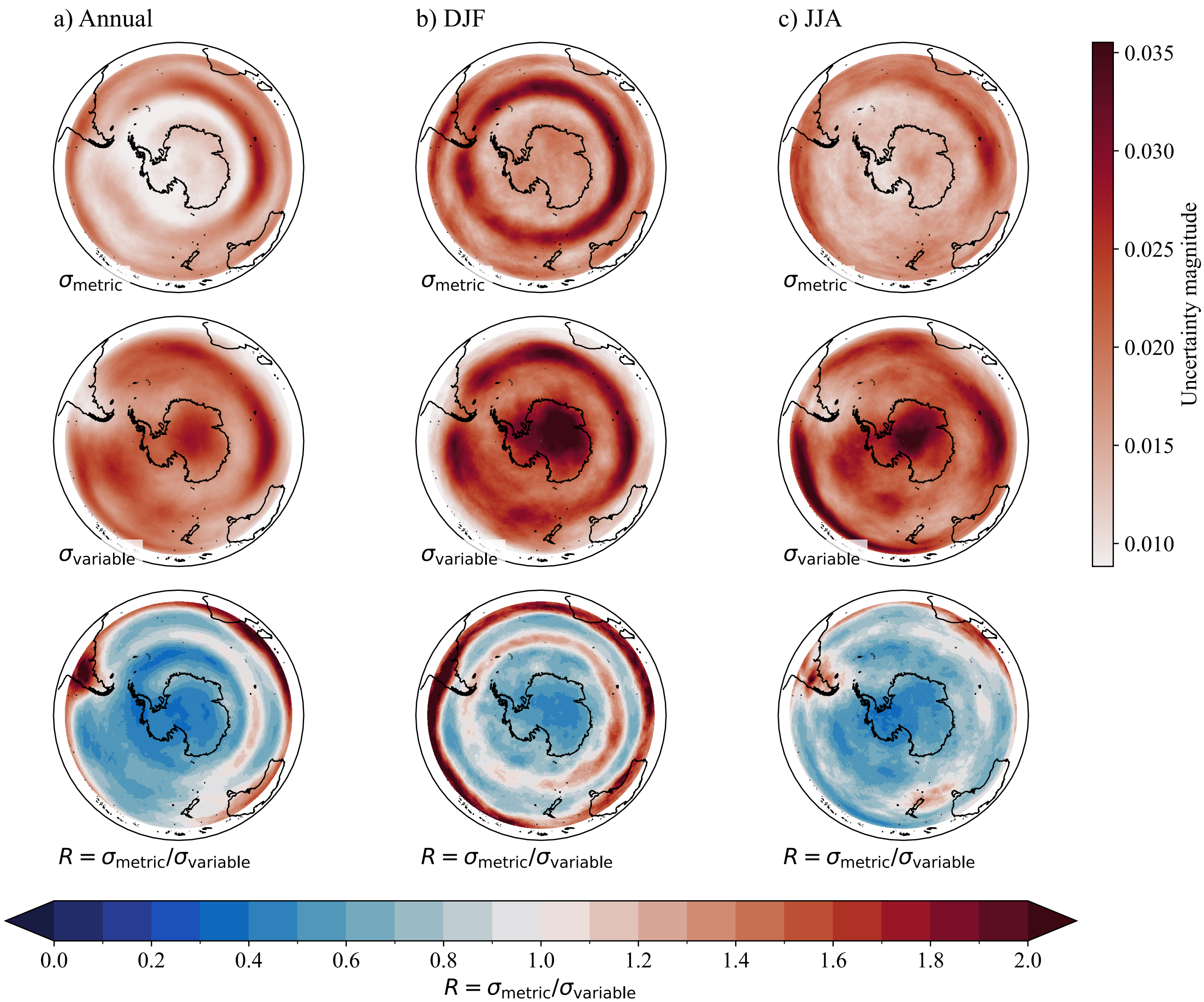

Figure 7: Spatial distribution of methodological uncertainty in Antarctic blocking detection. The top and middle row show
605 **uncertainty associated with the blocking metric (σ_{metric}) and diagnostic variable ($\sigma_{variable}$), respectively. The bottom row shows the dominance ratio R= σ_{metric} / $\sigma_{variable}$. Values below unity indicate that uncertainty is dominated by the choice of diagnostic variable, whereas values above unity indicate dominance by the choice of blocking metric. Results are shown for (a) the annual mean, (b) austral summer (DJF), and (c) austral winter (JJA).**

4.4 Blocking event characteristics

610 Figures 8 and 9 summarize the annual climatology of blocking event number, persistence, and intensity derived from the Z500- and PV-based detection methods, respectively. The results demonstrate that different blocking definitions lead to markedly different climatological patterns and event characteristics, reflecting the sensitivity of blocking diagnostics to the choice of variable and threshold logic. Rather than indicating the superiority of any single approach, these contrasts illustrate that

blocking is a definition-dependent phenomenon and that each method emphasizes different aspects of persistent circulation anomalies.

For the Z500-based methods (Fig. 8), the mean number of detected blocking events per year varies markedly among methodologies. The Z500-Abs and Z500-SD methods identify the largest number of events (Fig. 8b, c), whereas the Z500-Grad method identifies the fewest (Fig. 8a), reflecting fundamental differences in detection methods. The Z500-SD method is particularly sensitive to spatially extensive but moderate departures from the climatological background, allowing multiple distinct events to be identified over a given region, while the Z500-Perc method produces intermediate event counts by focusing on locally extreme and persistent anomalies.

Blocking persistence shows a different ordering among methods, with the threshold-based Z500 methods indicating greater persistence over the Antarctic continent than over the surrounding Southern Ocean (Fig. 8f-h). The Z500-Perc method produces the longest mean event durations, particularly over Antarctica, suggesting that once extreme anomalies relative to the local distribution are established, they can remain quasi-stationary for extended periods (Fig. 8h). The Z500-SD method shows intermediate persistence, while the Z500-Abs method yields shorter mean durations despite higher event counts, consistent with a tendency to fragment blocking activity into multiple shorter-lived events.

The corresponding diagnostics for the PV-based methods are shown in Fig. 9 and reveal some similarities with their Z500 counterparts when comparable thresholds are imposed (i.e., Abs, SD, and Perc), alongside contrasts between different methodological families. Overall, fewer blocking events are detected by PV-based methods than Z500-based methods, reflecting the more conservative nature of PV diagnostics and their focus on dynamically coherent circulation features. Blocking events detected by the PV-Abs and PV-SD methods show similar large scale spatial distributions, with enhanced event counts aligned along the outer edge of the polar vortex, while blocking detected by the PV-Perc method has the lowest event counts but the longest mean persistence. Persistence derived from vertically integrated PV shows less spatial variability than in the Z500-based methods, consistent with the reduced small-scale spatial variance of vertically integrated PV compared with single-level PV fields. Vertical integration over 150–500 hPa averages out PV anomalies confined to narrow layers, such as tropopause folds and PV streamers, while retaining anomalies that are coherent through a substantial depth of the upper troposphere and lower stratosphere.

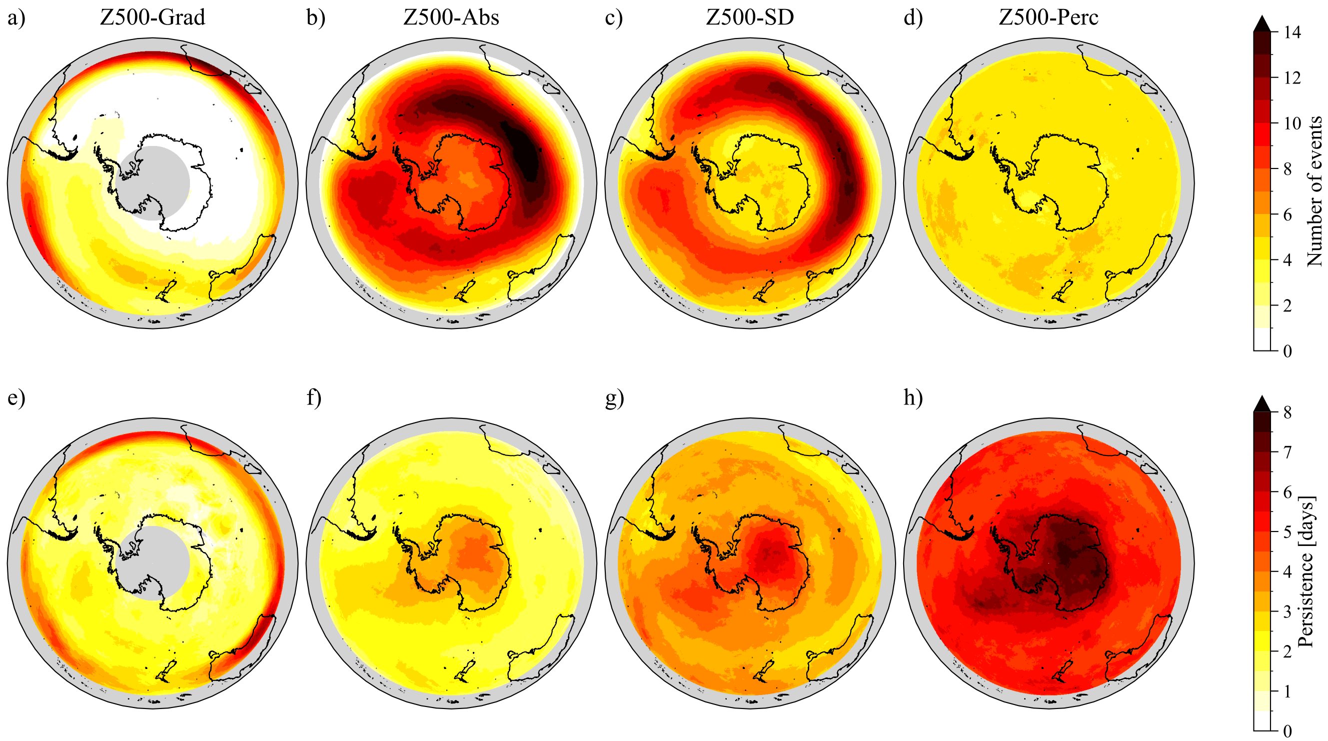

Figure 8: Annual climatology of blocking events derived from Z500-based detection methods. Panels a) to d) show the mean number of blocking events per year. Panels e) to h) show mean blocking persistence in days. Each column corresponds to one detection method, from left to right Z500 gradient, Z500 absolute, Z500 standard deviation-based anomaly, and Z500 percentile-based anomaly. Regions shown in gray correspond to latitudes where blocking detection is not applied (north of 25°S for all methods and south of 75°S for Z500-Grad).

Differences in event number and persistence point to a trade-off among detection methods. Methods yielding high event counts, such as Z500-Abs, tend to identify shorter-lived blocking features, suggesting sensitivity to a broader spectrum of positive anomalies rather than consolidated, quasi-stationary blocks. This behavior is consistent with earlier studies noting that some threshold-based methods may conflate true dynamical blocking with other persistent ridge structures (Tibaldi et al., 1997; Scherrer et al., 2006). In contrast, methods emphasizing flow reversal or local extremes tend to identify fewer but more persistent blocking events, more closely aligned with the canonical blocking paradigm reported in the early literature. Pronounced persistence over the Antarctic continent in percentile-based methods is consistent with studies showing that extreme geopotential height anomalies in high southern latitudes can remain anchored by topographic and thermal influences (Hoskins and Woollings, 2015; Clem et al. 2025).

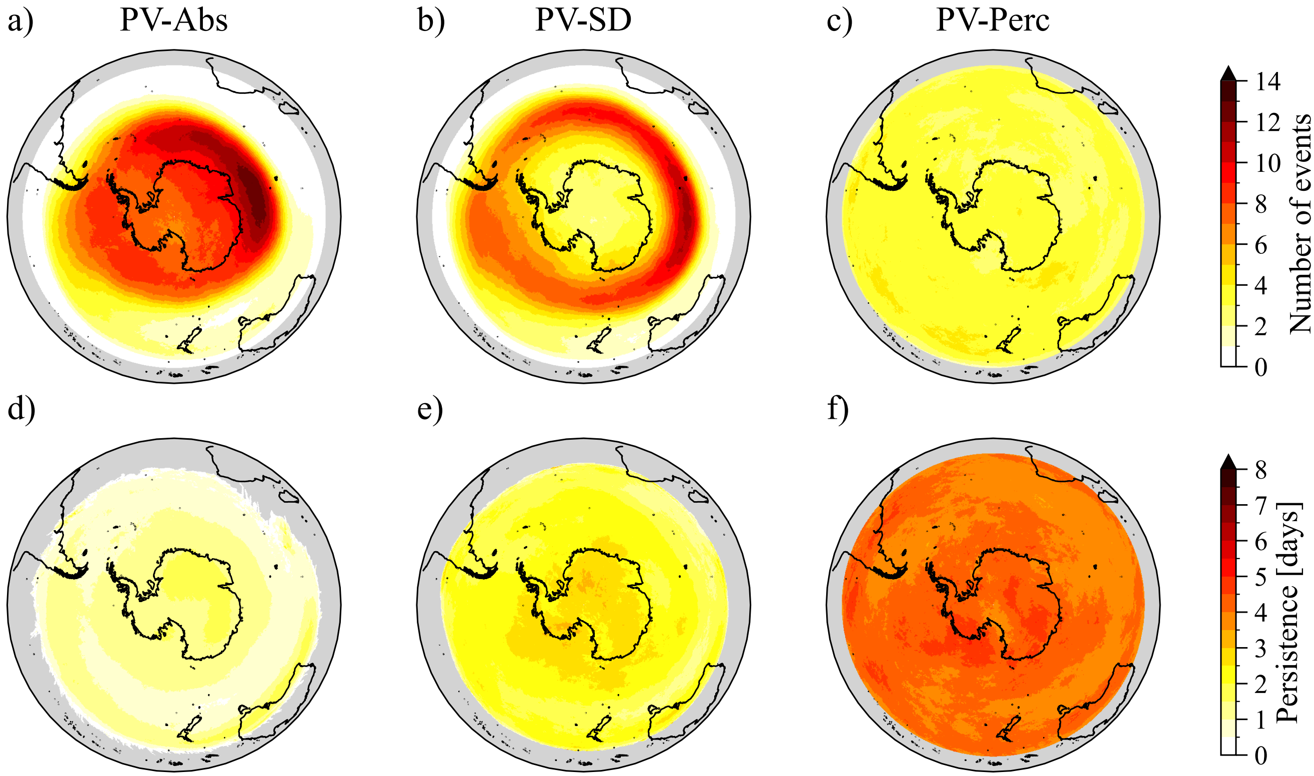

Figure 9: Annual climatology of blocking events derived from PV-based detection methods. Panels a) to c) show the mean number of blocking events per year. Panels d) to f) show mean blocking persistence in days. Each column corresponds to one detection method, from left to right PV absolute, PV standard deviation-based anomaly, and PV percentile-based anomaly. Regions shown in gray correspond to latitudes where blocking detection is not applied.

Blocking intensity is not analyzed here because its definition is inherently method dependent, particularly for absolute threshold approaches. For completeness, intensity diagnostics (excluding the absolute methods) are provided for both Z500 and PV, where they are used only to illustrate relative contrasts among anomaly-based metrics (Figs. S14 and S15).

PV-based diagnostics identify fewer and generally less persistent blocking events than Z500-based methods because they target a different dynamical signature. PV methods are specifically sensitive to large-scale wave breaking and potential vorticity streamer formation, processes that are typically more localized and transient than the broad, quasi stationary anticyclonic anomalies captured by height field methods (Hoskins et al., 1985; Berrisford et al., 2007). Within this framework, the PV-Perc method isolates the most extreme anomalies and yields the longest-lived events, suggesting that the most robust PV structures exhibit enhanced coherence and duration.

These diagnostics provide complementary perspectives on Antarctic blocking. The Z500-Grad method highlights canonical blocked flow patterns, anomaly-based Z500 methods emphasize regions of recurrent high-amplitude anomalies, and PV-based methods preferentially identify upper-tropospheric wave-breaking signatures. Together, they span a spectrum of persistent circulation regimes, from near-surface high pressure to upper-tropospheric and stratosphere–troposphere coupling events. These preliminary results underscore the value of a multi-diagnostic framework for synthesizing differing interpretations in the literature and for evaluating the representation of high-latitude blocking in climate models (Woollings et al., 2018; Hanna et al., 2024).

4.5 Case study comparison of blocking events

Figure 10 presents three representative blocking events from March 2015, February 2020, and March 2022, illustrating how the different methods capture the evolution and spatial structure of individual events. These periods correspond to well-documented Antarctic extreme events, including episodes over the Antarctic Peninsula (Bozkurt et al. 2018; Xu et al. 2021) and over East Antarctica (Wille et al. 2024a). For the threshold-based Z500 and PV methods, there is strong agreement on the timing and general location of blocking across all cases.

In March 2015 (Figs. 10a-c), the methods consistently identify a blocking structure over the Antarctic Peninsula, although the Z500-based methods delineate a broader region than the PV-based methods. In February 2020 (Figs. 10d-f), the underlying Z500-Abs, Z500-SD, and Z500-Perc masks initially identify a separate, short-lived anticyclonic ridge over the South Atlantic, east of South America. This feature does not merge with the blocking event over the Antarctic Peninsula and weakens at later time steps, while the Peninsula feature becomes more consolidated. In March 2022 (Figs. 10g-i), the PV-based methods identify a compact, dynamically coherent block near 90°–120°E, whereas the Z500 threshold methods capture a broader ridge signature.

Differences arise primarily in the delineation of event boundaries and spatial extent. The Z500-based threshold methods tend to produce larger and more expansive blocking regions, while the PV-based methods identify more compact blocked regions that closely follow the centers of the underlying dynamical anomalies. In all cases shown in Fig. 10, gradient-based features do not satisfy the minimum areal requirement applied uniformly across all methods and are therefore filtered out during event construction. When considered prior to areal filtering, the Z500-Grad method captures blocking-like structures associated with these events, but with spatial extents that are substantially smaller than those identified by threshold-based approaches (Fig. S16). Similar behavior has been reported in previous studies using alternative implementations of blocking diagnostics. For example, Wang et al. (2024) reported higher blocking frequencies when spatial constraints were relaxed. This comparison highlights the sensitivity of blocking diagnostics to methodological choices and the importance of applying spatial constraints to isolate large-scale features.

Despite these differences in spatial representation and sensitivity to areal filtering, the temporal evolution of the events detected by the threshold-based methods is highly consistent. The growth, mature, and decay phases of each block are captured coherently across each method, reinforcing confidence that the dataset presented here reliably represents the life cycle of major Antarctic blocking episodes. The case studies therefore demonstrate that methodological differences primarily influence the spatial characterization and quantitative metrics of blocking, while the identification of impactful large-scale events remains robust within the unified tracking framework.

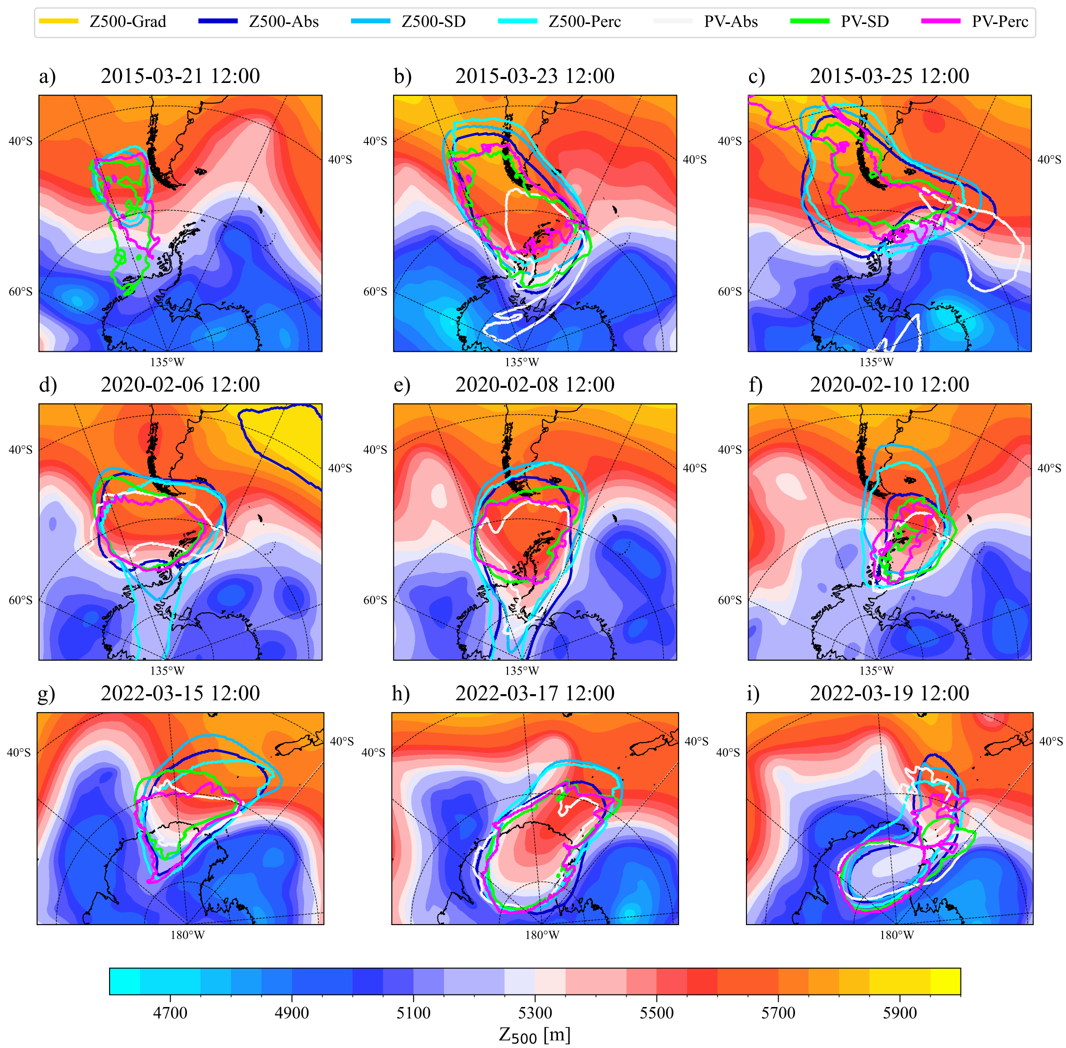

Figure 10: Comparison of blocking events detected by different methodologies for three representative cases. Panels a) to c) show the evolution of a blocking event in March 2015 over the Antarctic Peninsula, panels d) to f) show a blocking event in February 2020 over the Antarctic Peninsula, and panels g) to i) show a blocking event in March 2022 over East Antarctica. Colored contours indicate blocking regions detected by each method, as identified in the legend. Background color corresponds to 500 hPa geopotential height.

5 Data and Code Availability

The Antarctic blocking dataset presented in this study includes blocking masks, tracked events, climatological fields, and aggregated time series for all detection methods. The dataset is provided in NetCDF format with complete metadata and documentation to ensure transparency and reproducibility. All data products necessary to reproduce the results presented here are archived in the Zenodo repository: https://doi.org/10.5281/zenodo.18329806 (Bozkurt et al., 2026). The same repository also contains the preprocessing, detection, and event-tracking scripts used to generate the dataset, with the relevant parameter settings documented to facilitate reproduction and adaptation of the workflow.

The blocking detection and event tracking were performed using the TempestExtremes framework (Ullrich et al., 2021, https://github.com/ClimateGlobalChange/tempestextremes) together with custom preprocessing workflows developed for this study.

6 Conclusions and Outlook

This study presents a long-term dataset of Antarctic atmospheric blocking covering the period 1979–2024, derived from ERA5 reanalysis and constructed using multiple blocking detection methods applied consistently across the Southern Hemisphere. The dataset combines diagnostics based on 500 hPa geopotential height (Z500) and vertically integrated potential vorticity (PV, from 150–500 hPa) within a unified tracking and filtering framework, providing blocking masks, event catalogs, and climatological summaries that are directly comparable across methods and variables.

Across the range of detection approaches considered, Antarctic blocking exhibits methodological diversity in its diagnosed spatial extent, frequency, and persistence. Similarities are most evident between Z500- and PV-based methods that use comparable threshold formulations (Abs, SD, and Perc), which tend to identify similar major blocking episodes and broadly similar regions of occurrence. Beyond these method pairs, however, the blocking climatologies differ substantially, underscoring the strong dependence of Antarctic blocking characteristics on the chosen detection framework and definition. Diagnostics based on Z500 tend to capture a broader range of anticyclonic flow regimes, including events extending into the Antarctic interior, whereas PV-based diagnostics tend to identify fewer events that are more tightly associated with large-scale dynamical disturbances near the polar vortex. Event-based analyzes further reveal systematic trade-offs between event frequency and duration, reflecting how different methods emphasize either shorter-lived disturbances or more persistent blocking structures.

These contrasts reflect the fact that blocking at high southern latitudes can arise from multiple dynamical configurations that are captured differently by each method. Blocking may manifest through persistent anticyclonic circulation, upper-level disturbances interacting with the polar circulation, or combinations of both. As a result, no single blocking definition is universally optimal, and suitability depends on the application. Instead, the most appropriate approach depends on the research question: Z500-based methods appear best-suited for characterizing the broader footprint of persistent anticyclonic flow regimes and their surface impacts, whereas PV-based methods appear to provide a more dynamical perspective that isolates vertically coherent disturbances linked to wave breaking and polar-vortex variability. Within each variable, the Abs, SD, and Perc formulations emphasize different aspects of amplitude and local extremeness, while the gradient method provides a flow-geometry perspective but is more constrained by domain and areal filtering. The value of this blocking dataset is therefore not to rank the methods, but instead to enable users to quantify methodological uncertainty and to select a diagnostic matched to the aspect of blocking they wish to study.

Several limitations should be noted. First, blocking statistics remain sensitive to threshold choices, spatial filtering, and persistence criteria. Second, the application of uniform areal constraints may suppress smaller-scale features. Finally, the dataset relies on a single reanalysis product, which may influence the representation of blocking in earlier decades and over data-sparse regions of Antarctica and the Southern Ocean. Sensitivity experiments show that the retained parameter choices provide a physically coherent balance between widespread detection of weak or transient ridging and overly restrictive detection of only the strongest anomalies. For the gradient method, more permissive settings increase continental detections but may also introduce dynamically ambiguous features. We therefore retain Z500-Grad as a conservative flow geometry baseline. Its weak detection over the Antarctic interior is informative because it provides a reference against which the broader anomaly-based methods can be compared, rather than evidence that blocking is absent from the region. Redefining the latitudinal bands would constitute a distinct polar adapted reversal method that requires dedicated physical validation. Development and validation of a reversal diagnostic adapted to the polar region remain important priorities for future work.

Looking ahead, the framework presented here can be extended to other reanalysis products and to climate model output to assess the robustness of blocking characteristics, their representation in models, and projected changes under future climate scenarios (e.g. Patterson et al., 2019). Beyond event-focused analyzes, the dataset provides a consistent basis for examining the role of atmospheric blocking within broader modes of Southern Hemisphere variability and large-scale teleconnection patterns, including links to tropical forcing, stratospheric variability, and annular circulation changes. By enabling blocking to be studied alongside related processes such as atmospheric rivers, warm air intrusions, surface melt events, and sea ice variability, this dataset supports integrated investigations of Antarctic circulation variability and its evolution under climate forcing. Making these data publicly available, together with transparent documentation of the underlying methodology, is intended to facilitate reproducible research and to support continued progress in understanding the Antarctic climate system. The dataset has been designed to be extensible and to facilitate future updates as new reanalysis data become available. While the present release covers the period 1979–2024, the underlying workflow allows the dataset to be updated on a regular basis, enabling continued extension in time and ensuring long-term relevance for studies of Antarctic circulation variability and extreme events.

Author contributions

This study was developed through collaborative discussions among all authors. DB and CO coordinated the dataset development in close collaboration with the full project team, implemented the blocking detection and tracking framework, and carried out the analyzes. DB led the manuscript preparation with contributions from CO. All authors participated in reviewing, editing, and revising the manuscript.

Competing interests

The authors declare that they have no conflict of interest.

Acknowledgments

We acknowledge the Copernicus Climate Change Service (C3S) Climate Data Store for providing the ERA5 reanalysis data used in this study. Powered@NLHPC: This research was partially supported by the supercomputing infrastructure of the NLHPC (CCSS210001). We thank Paul Ullrich (University of California, Davis) and Burcu Boza (Istanbul Technical University) for helpful discussions regarding the use of TempestExtremes in this work.

Funding

D.B. acknowledges support from ANID-FONDECYT-1240190, ANID-FONDAP-1523A0002, COPAS COASTAL ANID FB210021, and ANID ANILLO ATE250008. V.F. and V.B acknowledge the support from the Agence Nationale de la Recherche (ANR) through the project ANR-20-CE01-0013 623 (ARCA). K.R.C. acknowledges support from ANID-FONDECYT-1240190 for a research stay at the University of Valparaíso, Department of Meteorology, which contributed to this work. J.C.M. acknowledges support from ANID-FONDECYT-1252128.

References

American Meteorological Society (AMS), 2026: “Blocking high.” Glossary of Meteorology, https://glossary.ametsoc.org/wiki/blocking-high/, last access: 21 June 2026.

Baiman, R., Winters, A.C., Pohl, B. et al. Synoptic and planetary-scale dynamics modulate Antarctic atmospheric river precipitation intensity. Commun. Earth Environ. 5, 127. https://doi.org/10.1038/s43247-024-01307-9, 2024.

Barnes, E. A., Dunn-Sigouin, E., Masato, G., and Woollings, T.: Exploring recent trends in Northern Hemisphere blocking, Geophys. Res. Lett., 41, 638–644, 2014.

Barrett, B. S., Lafluer, D.M., and Henderson, G.R.: Madden–Julian Oscillation modulation of Antarcic sea ice. *Glacies*, 2(4), 16, https://doi.org/10.3390/glacies2040016, 2025.

Barriopedro, D., García-Herrera, R, Lupo, A. R., and Hernández, E.: A Climatology of Northern Hemisphere Blocking. J. Climate, 19, 1042–1063, https://doi.org/10.1175/JCLI3678.1, 2006.

Berrisford, P., Hoskins, B. J., and Tyrlis, E.: Blocking and Rossby wave breaking on the dynamical tropopause in the Southern Hemisphere, *J. Atmos. Sci.*, 64, 2881–2898, https://doi.org/10.1175/JAS3984.1, 2007.

Bozkurt, D., Opazo, C., Marín, J. C., Clem, K. R., Pohl, B., Buffet, V., Favier, V., Carrasco-Escaff, T., and Barrett, B. S.: A multi-method Antarctic atmospheric blocking dataset based on ERA5 (1979–2024), Zenodo [data set], https://doi.org/10.5281/zenodo.18329807, 2026.

Bozkurt, D., Marín, J., Barrett, B.: Temperature and moisture transport during atmospheric blocking patterns around the Antarctic Peninsula, *Weather Clim. Extrem.*, 38, 100506, https://doi.org/10.1016/j.wace.2022.100506, 2022.

Bozkurt, D., Marín, J., Verdugo, C., and Barrett, B.: Atmospheric blocking and temperatures in the Antarctic Peninsula, *Sci. Total Environ.*, 931, 172852, https://doi.org/10.1016/j.scitotenv.2024.172852, 2024.

Bozkurt, D., Rondanelli, R., Marín, J., and Garreaud, R.: Foehn event triggered by an atmospheric river underlies record-setting temperature along continental Antarctica, *J. Geophys. Res.-Atmos.*, 123, 3871–3892, https://doi.org/10.1002/2017JD027796, 2018.

Carrera, M. L., Higgins, R. W., and Kousky, V. E.: Downstream weather impacts associated with atmospheric blocking over the Northeast Pacific, *J. Climate*, 17, 4823–4839, https://doi.org/10.1175/JCLI-3237.1, 2004.

Clem, K. R., MacFerrin, M., Kennett, D., Bozkurt, D., and Scambos, T.: Record warmth and surface melt on the Antarctic Peninsula in February 2020, *Bull. Amer. Meteor. Soc.*, 102, S328–S329, https://doi.org/10.1175/BAMS-D-21-0081.1, 2021.

Clem, K. R., Bozkurt, D., Kennett, D., King, J. C., and Turner, J.: Central tropical Pacific convection drives extreme high temperatures and surface melt on the Larsen C Ice Shelf, Antarctic Peninsula, *Nat. Commun.*, 13, 3906, https://doi.org/10.1038/s41467-022-31119-4, 2022.

Clem, K. R., Batzli, S., Bozkurt, D., et al. Meteorology and Climate of Antarctica. In: Taschetto AS, Ndarana T, Ambrizzi T, eds. Meteorology and Climate of the Southern Hemisphere. Cambridge University Press, 241-283, https://doi.org/10.1017/9781009352680.009, 2025.

Davini, P., Cagnazzo, C., Neale, R., and Tríbbia, J.: Coupling between Greenland blocking and the North Atlantic Oscillation pattern, *Geophys. Res. Lett.*, 39, L14801, https://doi.org/10.1029/2012GL052315, 2012.

Dole, R. M.: The life cycle of persistent anomalies and blocking over the North Pacific, *Adv. Geophys.*, 29, 31–69, 1986.

Dole, R. M., and Gordon, N. D.: Persistent anomalies of the extratropical Northern Hemisphere wintertime circulation: Geographical distribution and regional persistence characteristics, *Mon. Weather Rev.*, 111, 1567–1586, https://doi.org/10.1175/1520-0493(1983)111<1567:PAOTEN>2.0.CO;2, 1983.

Dong, L. and Colucci, S.J.: The role of deformation and potential vorticity in Southern Hemisphere blocking onsets. J. Atmos. Sci., 62(11), .4043-4056, https://doi.org/10.1175/JAS3576.1, 2005.

Fogt, R. L., Jones, J. M., and Renwick, J.: Seasonal zonal asymmetries in the Southern Annular Mode and their impact on regional temperature anomalies, *J. Climate*, 25, 6253–6270, https://doi.org/10.1175/JCLI-D-11-00474.1, 2012.

Francis, D., Fonseca, R., Nelli, N., Heil, P., Wille, J., Gorodetskaya, I., and Massom, R.: Impacts of atmospheric dynamics on sea-ice and snow thickness at a coastal site in East Antarctica, *EGUsphere* [preprint], https://doi.org/10.5194/egusphere-2024-3535, 2025.

Gilbert, E., Pishniak, D., Torres, J. A., Orr, A., Maclennan, M., Wever, N., and Verro, K.: Extreme precipitation associated with atmospheric rivers over West Antarctic ice shelves, *The Cryosphere*, 19, 597–618, https://doi.org/10.5194/tc-19-597-2025, 2025.

Gorodetskaya, I. V., Tsukernik, M., Claes, K., Ralph, M. F., Neff, W. D., and van Lipzig, N. P. M.: The role of atmospheric rivers in anomalous snow accumulation in East Antarctica, *Geophys. Res. Lett.*, 41, 6199–6206, https://doi.org/10.1002/2014GL060881, 2014.

Gorodetskaya, I. V., Durán-Alarcón, C., González-Herrero, S., Clem, K. R., Zou, X., Rowe, P., et al.: Record-high Antarctic Peninsula temperatures and surface melt in February 2022, *npj Clim. Atmos. Sci.*, 6, 202, https://doi.org/10.1038/s41612-023-00529-6, 2023.

Grotjahn, R., Black, R., Leung, R., et al.: North American extreme temperature events and related large-scale meteorological patterns, *Clim. Dyn.*, 46, 1151–1184, https://doi.org/10.1007/s00382-015-2638-6, 2016.

Hanna, E., Francis, J., Wang, M., et al.: Influence of high-latitude blocking and the northern stratospheric polar vortex on cold-air outbreaks, *Environ. Res.: Clim.*, 3, 042004, https://doi.org/10.1088/2752-5295/ad93f3, 2024.

Henderson, G.R., Barrett, B. S., Lois, A., and Elsaawy, H.: Time-lagged response of the Antarctic atmosphere to tropical MJO convection. *Mon. Wea. Rev.*, 146, 1219-1231, https://doi.org/10.1175/MWR-D-17-0224.1, 2018.

Henderson, G.R., Barrett, B.S., Wachowicz, L.J., Mattingly, K.S., Preece, J.R. and Mote, T.L.: Local and remote atmospheric circulation drivers of Arctic change: A review. *Front. Earth Sci.*, 9, p.709896, https://doi.org/10.3389/feart.2021.709896, 2021.

Hauser, S., Teubler, F., Riemer, M., Knippertz, P., and Grams, C. M.: Life cycle dynamics of Greenland blocking from a potential vorticity perspective, *Weather Clim. Dynam.*, 5, 633–658, https://doi.org/10.5194/wcd-5-633-2024, 2024.

Hauser, S., Teubler, F., Riemer, M., and Grams, C. M.: A quasi-Lagrangian perspective on the role of dry and moist processes in the formation of blocked North Atlantic–European weather regimes, *Weather Clim. Dynam.*, 7, 937–958, https://doi.org/10.5194/wcd-7-937-2026, 2026.

Hersbach, H., Bell, B., Berrisford, P., et al.: The ERA5 global reanalysis, *Quart. J. Roy. Meteor. Soc.*, 146, 1999–2049, https://doi.org/10.1002/qj.3803, 2020.

Hoffmann, L. and Spang, R.: An assessment of tropopause characteristics of the ERA5 and ERA-Interim meteorological reanalyses, *Atmos. Chem. Phys.*, 22, 4019–4046, https://doi.org/10.5194/acp-22-4019-2022, 2022.

Hoskins, B. J., McIntyre, M. E., and Robertson, A. W.: On the use and significance of isentropic potential vorticity maps, *Quart. J. Roy. Meteor. Soc.*, 111, 877–946, https://doi.org/10.1002/qj.49711147002, 1985.

Hoskins, B., & Woollings, T.: Persistent Extratropical Regimes and Climate Extremes. Current Climate Change Reports, 1(3), 115-124, 2015.

Liang, K., Wang, J., Luo, H., and Yang, Q.: The role of atmospheric rivers in Antarctic sea ice variations, *Geophys. Res. Lett.*, 50, e2022GL102588, https://doi.org/10.1029/2022GL102588, 2023.

Lim, E.-P., Thompson, D. W. J., Butler, A. H., Wheeler, M. C., Nakamura, H., Jucker, M., Arblaster, J. M., Hendon, H. H., Newman, P. A., and Coy, L.: Characteristics of Antarctic stratospheric variability during winter: A case study of the 2024 sudden stratospheric warming and its surface impacts, *J. Geophys. Res. Atmos.*, 131, e2025JD045089, https://doi.org/10.1029/2025JD045089, 2026.

Liu, Z., and Wang, L.: Enhanced occurrence of atmospheric blocking in the Southern Hemisphere by baroclinic annular mode, *Geophys. Res. Lett.*, 51, e2023GL107343, https://doi.org/10.1029/2023GL107343, 2024.

Maclennan, M. L., Lenaerts, J. T. M., Shields, C. A., et al.: Climatology and surface impacts of atmospheric rivers on West Antarctica, *The Cryosphere*, 17, 865–881, https://doi.org/10.5194/tc-17-865-2023, 2023.

Marín, J., Bozkurt, D., and Barrett, B.: Atmospheric blocking trends and seasonality around the Antarctic Peninsula, *J. Climate*, 35, 3803–3818, https://doi.org/10.1175/JCLI-D-21-0323.1, 2022.

Marshall, G.J. and King, J.C.: Southern Hemisphere circulation anomalies associated with extreme Antarctic Peninsula winter temperatures. *Geophys. Res.. Lett.*, 25(13), 2437-2440, https://doi.org/10.1029/98GL01651, 1998.

Marshall, G. J., Orr, A., van Lipzig, N. P. M., and King, J. C.: The impact of a changing Southern Hemisphere annular mode on Antarctic Peninsula summer temperatures, *J. Climate*, 19, 5388–5404, https://doi.org/10.1175/JCLI3844.1, 2006.

Masato, G., Hoskins, B. J., and Woollings, T.: Wave-breaking characteristics of Northern Hemisphere winter blocking, *J. Climate*, 26, 4535–4549, https://doi.org/10.1175/JCLI-D-12-00240.1, 2013.

Nakamura, N., and Huang, C. S. Y.: Atmospheric blocking as a traffic jam in the jet stream, *Science*, 361, 42–47, https://doi.org/10.1126/science.aat0721, 2018.

Patterson, M., Bracegirdle, T., and Woollings, T.: Southern Hemisphere atmospheric blocking in CMIP5 and future changes in the Australia–New Zealand sector, *Geophys. Res. Lett.*, 46, 9281–9290, https://doi.org/10.1029/2019GL083264, 2019.

Pepler, A.: Projections of synoptic anticyclones for the twenty-first century, *Clim. Dyn.*, 61, 3271–3287, https://doi.org/10.1007/s00382-023-06728-4, 2023.

Pinheiro, M. C., Ullrich, P. A., and Grotjahn, R.: Atmospheric blocking and intercomparison of objective detection methods, *Clim. Dyn.*, 53, 4189–4216, https://doi.org/10.1007/s00382-019-04782-5, 2019.

Ploeger, F., Diallo, M., Charlesworth, E., Konopka, P., Legras, B., Laube, J. C., Grooß, J.-U., Günther, G., Engel, A., and Riese, M.: The stratospheric Brewer–Dobson circulation inferred from age of air in the ERA5 reanalysis, *Atmos. Chem. Phys.*, 21, 8393–8412, https://doi.org/10.5194/acp-21-8393-2021, 2021.

Pohl, B., Favier, V., Wille, J., et al: Relationship between weather regimes and atmospheric rivers in East Antarctica, *J. Geophys. Res. Atmos.*, 126, e2021JD035294. https://doi.org/10.1029/2021JD035294, 2021.

Polster, C., and Wirth, V.: A new atmospheric background state to diagnose local waveguidability, *Geophys. Res. Lett.*, 50, e2023GL106166, https://doi.org/10.1029/2023GL106166, 2023.

Renwick, J. A.: ENSO-related variability in the frequency of South Pacific blocking, *Mon. Weather Rev.*, 126, 3117–3123, https://doi.org/10.1175/1520-0493(1998)126<3117:ERVITF>2.0.CO;2, 1998.

Renwick, J. A., and Revell, M. J.: Blocking over the South Pacific and Rossby wave propagation, *Mon. Weather Rev.*, 127, 2233–2247, https://doi.org/10.1175/1520-0493(1999)127<2233:BOTSPA>2.0.CO;2, 1999.

Rex, D. F.: Blocking action in the middle troposphere and its effect upon regional climate, *Tellus*, 2, 196–211, https://doi.org/10.1111/j.2153-3490.1950.tb00331.x, 1950.

Rondanelli, R., Hatchett, B., Rutllant, J., Bozkurt, D., and Garreaud, R.: Strongest MJO on record triggers extreme Atacama rainfall and warmth in Antarctica, *Geophys. Res. Lett.*, 46, 3482–3491, https://doi.org/10.1029/2018GL081475, 2019.

Scherrer, S. C., Croci-Maspoli, M., Schwierz, C., and Appenzeller, C.: Two-dimensional indices of atmospheric blocking, *Int. J. Climatol.*, 26, 233–249, https://doi.org/10.1002/joc.1250, 2006.

Schwierz, C., Croci-Maspoli, M., and Davies, H. C.: Perspicacious indicators of atmospheric blocking, *Geophys. Res. Lett.*, 31, L06125, https://doi.org/10.1029/2003GL019341, 2004.

Sousa, P. M., Barriopedro, D., García-Herrera, R., Woollings, T., and Trigo, R. M.: A new combined detection algorithm for blocking and subtropical ridges, *J. Climate*, 34, 7735–7758, https://doi.org/10.1175/JCLI-D-20-0658.1, 2021.

Tang, H., Li, S., Jones, J.M. et al.: Unprecedented 2024 East Antarctic winter heatwave driven by polar vortex weakening and amplified by anthropogenic warming. *npj Clim Atmos Sci* 9, 122, https://doi.org/10.1038/s41612-026-01392-x, 2026.

Tibaldi, S., and Molteni, F.: On the operational predictability of blocking. *Tellus*, 42A, 343–365, https://doi.org/10.3402/tellusa.v42i3.11882, 1990.

Tibaldi, S., Tosi, E., Navarra, A., and Pedulli, L.: Northern and Southern Hemisphere seasonal variability of blocking frequency, *Mon. Weather Rev.*, 122, 1971–2003, https://doi.org/10.1175/1520-0493(1994)122<1971:NASHSV>2.0.CO;2, 1994.

Tibaldi, S., D'Andrea, F., Tosi, E., and Roeckner, E.: Climatology of the northern hemisphere blocking in the ECHAM model, *Clim. Dyn.*, 13, 649-666, 1997.

Trenberth, K. E., and Mo, K. C.: Blocking in the Southern Hemisphere, *Mon. Weather Rev.*, 113, 3–21, https://doi.org/10.1175/1520-0493(1985)113<0003:BITSH>2.0.CO;2, 1985.

Turner, J., Lu, H., King, J. C., Carpentier, S., Lazzara, M., Phillips, T., and Wille, J.: An extreme high temperature event in coastal East Antarctica associated with an atmospheric river and record summer downslope winds, *Geophys. Res. Lett.*, 49(4), e2021GL097108. https://doi.org/10.1029/2021GL097108, 2022.

Ullrich, P. A., Zarzycki, C. M., McClenny, E. E., et al.: TempestExtremes v2.1, *Geosci. Model Dev.*, 14, 5023–5048, https://doi.org/10.5194/gmd-14-5023-2021, 2021.

Wachowicz, L., Preece, J., Mote, T., Barrett, B.S., Henderson, G.R.: Historical trends of seasonal Greenland blocking under different blocking metrics. *Int. J. Clim*., 41, E3263-E3278, https://doi.org/10.1002/joc.6923, 2021.

Wang, G., Hendon, H.H., Arblaster, J.M., Lim, E.-P., Abhik, S., and van Rensch, P.: Compounding Tropical and Stratospheric Forcing of the Record Low Antarctic Sea-Ice in 2016. *Nat. Commun*, 10, 13, https://doi.org/10.1038/s41467-018-07689-7, 2019.

Wang, S., Ding, M., Liu, G., Li, G., and Chen, W.: Blocking events in East Antarctica, *J. Climate*, 37, 1333–1345, https://doi.org/10.1175/JCLI-D-23-0419.1, 2024.

Wille, J. D., and Coauthors: The extraordinary March 2022 East Antarctica heat wave, *J. Climate*, 37, 757–778, https://doi.org/10.1175/JCLI-D-23-0175.1, 2024a.

Wille, J. D., and Coauthors: Examining atmospheric river life cycles in East Antarctica, *J. Geophys. Res. Atmos.*, 129, e2023JD039970, https://doi.org/10.1029/2023JD039970, 2024b.

Wille, J. D., Favier, V., Jourdain, N. C., et al.: Intense atmospheric rivers can weaken ice shelf stability, *Commun. Earth Environ.*, 3, 90, https://doi.org/10.1038/s43247-022-00422-9, 2022.

Wille, J., Favier, V., Gorodetskaya, I., et al.: Atmospheric rivers in Antarctica, *Nat. Rev. Earth Environ.*, 6, 178–192, https://doi.org/10.1038/s43017-024-00638-7, 2025.

Woollings, T., Barriopedro, D., Methven, J., et al.: Blocking and its response to climate change, *Curr. Clim. Change Rep.*, 4, 287–300, https://doi.org/10.1007/s40641-018-0108-z, 2018.

Xu, M., Yu, L., Liang, K., Vilma, T., Bozkurt, D., Hu, X., and Yang, Q.: Dominant role of vertical air flows in the unprecedented warming on the Antarctic Peninsula, *Commun. Earth Environ.*, 2, 133, https://doi.org/10.1038/s43247-021-00203-w, 2021.

Zhai, Z., Wang, Y., Wu, Q., and Hou, S.: Record-breaking warm late winter over Antarctica in 2024, *Geophys. Res. Lett.*, 52, e2024GL114528, https://doi.org/10.1029/2024GL114528, 2025.